Optical Properties of II-VI Compound Semiconductor Quantum Dots in Polyvinyl Alcohol

Jifa Qi

A dissertation submitted to the Doctoral Program
in Physics, the University of Tsukuba
in partial fulfilment of the requirements for the
degree of Doctor of Science

December, 1996

Abstract

Quantum dots (quasi-zero-dimensional electron systems) are one class of the most interesting system in semiconductor nanostructures and have received considerable attention in the past decade. Besides being an interesting physical system where new physical phenomena are expected to be explored, quantum dots are also interesting from the technological point of views. In this research, the optical properties of II-VI compound semiconductor quantum dots in a polymer matrix were investigated. We prepared CdS and CdS:Mn quantum dots embedded in polyvinyl alcohol (PVA) matrix through chemical methods and investigated their optical properties by means of optical absorption, photoluminescence, time-resolved photoluminescence, photoluminescence excitation, time-resolved optical absorption, nanosecond pump-probe and persistent spectral hole burning (PSHB) measurements.

We first studied the PSHB phenomena in CdS quantum dots embedded in the polymer matrix and found that its persistent time depends on the molar ratio of Cd^{2+}/S^{2-} in the sample. It is found that the persistent time of burnt hole is less than 0.33 ms when the molar ratio of Cd^{2+}/S^{2-} is less than 1, less than 0.1 sec when Cd^{2+}/S^{2-} is near 1, and larger than 1 min when Cd^{2+}/S^{2-} is larger than 1. Based on the experimental observations, we proposed an electron photoionization model to explain why the PSHB phenomena are observed in quantum dots. When a quantum dot is excited, an electron escapes from the quantum dot through the potential barrier in the polymeric matrix and is trapped at Cd^{2+} center in the polymeric matrix. Photoionized quantum dots and trapped electrons are stable enough to give PSHB at

low temperatures. There are many spatial configurations for electrons and holes in both quantum dots and the polymeric host. A variety of spatial arrangements induce an additional inhomogeneous broadening of the absorption spectra of CdS quantum dot. The presence of the inhomogeneous broadening due to the carrier spatial distribution satisfies the requirement of the PSHB.

We studied the magnetic ion Mn^{2+} doped CdS quantum dots, since physical properties of semiconductors are greatly influenced by the doped impurities. CdS:Mn quantum dots belong to a new kind system —diluted magnetic semiconductor quantum dots. Similar to CdS quantum dots, the blue-shifted absorption spectrum due to the quantum size effect was observed also in the CdS:Mn quantum dots. The intense luminescence from Mn^{2+} was observed. It shows a large quantum yield of 20%, and decays very fast with a nanosecond order of lifetimes which is shorter than the corresponding one of millisecond order of lifetime in bulk CdS:Mn crystals by five orders of magnitude. From the photoluminescence excitation spectrum, we found that Mn^{2+} is excited through the energy transfer from photoexcited CdS quantum dots. The doped Mn^{2+} ions are located in the quantum dots, or on the surface of the quantum dots and outside the quantum dots in the matrix. MnS compounds are formed by the Mn^{2+} ions located on the surface and in the polymer matrix. Since the band gap of MnS crystal (3.75 eV) is much wider than the band gap of CdS quantum dots, MnS cannot be excited by the photons with the energies less than 3.492 eV (which is the maximum photon energy we used to excite CdS quantum dots). MnS on the surface of quantum dots may moderate the defect of quantum dots, decrease the nonradiative energy transfer to the surface trap centers. So that the Mn^{2+} photoluminescence is from the Mn^{2+} ion $^4T_1 - {}^6A_1$

transition in the CdS host quantum dots. Large mixing of exciton state of CdS with the d state of Mn^{2+} makes an effective energy transfer path from CdS to Mn^{2+} (through the exchange interaction and electric multipole interaction), relaxes the partial spin-forbidden Mn^{2+} cations, and results in a fast decay time of Mn^{2+}. The observed high quantum yield is considered as due to the decrease of the nonradiative relaxation rate, the increase of the energy transfer rate from CdS to Mn^{2+} and the increase of the radiative rate of Mn^{2+}.

Contents

1 Introduction

Nanometer semiconductor crystallites or semiconductor quantum dots have attracted much attention in recent years in the field of physics, chemistry, material sciences, electronic engineering and technology. Optical and electronic properties of quantum dots are of special interests, because they exhibit new quantum phenomena and have potential applications for the novel devices [1]. When the sizes of nanometer semiconductors are small compared to the exciton Bohr radius of bulk semiconductor, their electronic wave-functions undergo a three-dimensional quantum confinement due to the quantum dot boundary. The confinement effect induces the quantization of the electronic bands, so that the quantum dots have discrete electronic transitions shifting to higher energies with the decrease of the size. On the other hand, the physical properties of semiconductor are greatly influenced by the doped impurities, the magnetic ion doped quantum dots (diluted magnetic semiconductor quantum dots) have attracted attentions recently because they can combine both the semiconductor nanometer size confinement effect and magnetic finite size effects.

So far, a variety of methods have been used to fabricate the free standing semiconductor quantum dots, and the quantum dots embedded in crystal, glass, polymer, solution and porous materials, and much effort was spent to make size monodispersed and surface perfect. The studies of optical properties of I-Ⅶ, Ⅱ-Ⅵ, Ⅲ-Ⅴ, et al., compound semiconductor and Ⅳ element semiconductor quantum dots have been reported. For example, the major parts of works have been done in CdS [1-6], CdSe [7-10], CdS_xSe_{1-x} [11], CdTe [12-14], CuCl or CuBr [15-16], GaAs, InP, or InAs [17-21], and Si related quantum structure materials [22].

In this research, we have prepared the Ⅱ - Ⅵ compound semiconductor CdS, CdSe, ZnSe and CdS:Mn, CdSe:Mn, ZnSe:Mn quantum dots through the polymer organmetallic chemical methods, and studied the optical properties of them by means of optical absorption, photoluminescence, photoluminescence excitation, time-resolved photoluminescence and nanosecond pump-probe measurements.

The contents of this paper are organized as follows. In Section 1, we describe the fundamental physics of this paper: the semiconductor quantum dots, the diluted magnetic semiconductor quantum dots, and the related material features of CdS and CdS:Mn. In Section 2, we simply review the synthesis methods of the quantum dots, and describe our method of preparing CdS, CdSe, ZnSe and CdS:Mn, CdSe:Mn, ZnSe:Mn quantum dots embedded in polyvinyl alcohol. In Section 3, we give the observation results on persistent spectral hole burning in CdS quantum dots, and propose a possible mechanism based on the observations. In Section 4, we report the luminescence properties of CdS:Mn quantum dot, make the comparisons with CdS quantum dots embedded in polyvinyl alcohol and the bulk CdS:Mn crystal, and propose the possible mechanism to explain the novel optical properties of CdS:Mn quantum dots. Finally, in Section 5, we give the conclusion of this research and remarks on future study.

In the following parts of this section, we present a brief background of quantum dot, diluted magnetic semiconductor and the material properties of CdS, CdS:Mn crystals and quantum dots.

1.1 Semiconductor quantum dot

Most of the electronic elementary excitations in solids possess a spatial extension several times larger than the lattice constant of the crystal. The rapid development of technology enables the fabrication of confined semiconductor structures of low dimensions to be realizable on the nanometer scale. Depending on the confinement geometry, these structures have been classified into two-dimensional (quantum wells), one-dimensional (quantum wires), and zero-dimensional (quantum dots) systems (see Fig. 1.1).

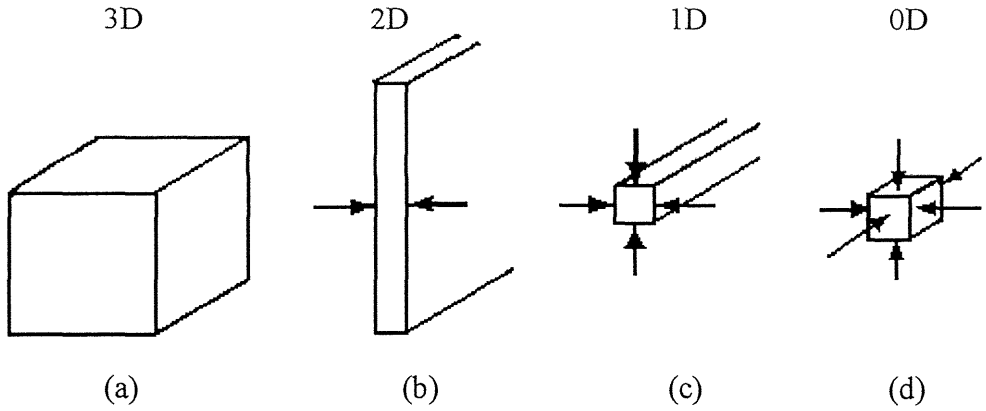

Fig. 1.1 Geometric illustrations of material system of different dimensionality: (a) bulk semiconductor, 3D; (b) quantum wells, 2D; (c) quantum wires, 1D; (d) quantum dots, 0D.

In semiconductor quantum structures, such as quantum wells, quantum wires and quantum dots, the most drastic change due to the quantum confinement effect is the quantization of the electronic bands, so that the quantum structures have the discrete electronic transitions shifting to higher energies with the decrease of the size. Especially in quantum dots, this change can be easily observed through the optical

absorption spectrum that shows a blue shift of the absorption edge as the size is reduced. As a result, the optical absorption spectroscopy is widely used in the study of the quantum size effect of dots. The absorption edge of direct and allowed semiconductors is governed by the exciton absorption. Depending on the average quantum dot radius R, the confinement effects can be divided into three regimes: the weak confinement regime ($R >> a_B$), the strong confinement ($R << a_B$) and the intermediate confinement regime, where a_B is the exciton Bohr radius of bulk crystal. The excitons of different confinement regimes in the quantum dots will be stated in later part of this section.

In spite of a number of common properties for all of these quantum-confined systems, there are several interesting features inherent in quasi-zero-dimensional structures. Quantum wells and quantum wires still possess a translational symmetry in two or one dimension, semiconductor quantum dots do not possess the translational symmetry in all directions (with quantum dot system, there is confinement in all three dimensions). Unlike quantum wells or quantum wires, quantum dots are hardly to study by means of electric techniques, and contactless optical methods are used to study the electronic properties of these structures, especially, if the quantum dots are embedded in an insulating matrix. Some preparation methods for quantum dots in transparent host materials are quite different from those for the quantum wells or quantum wires, and some of them are very old of the history of centuries.

Since the first concept of zero-dimensional structures has been published in the early eighties [23-25], a large progress has been achieved [1]. The research of the quantum dot has been developed as a

separated field bordered by solid state physics, colloidal chemistry, laser physics and optics. The investigated quantum dot systems include the microcrystallites, nanocrystals, clusters and colloids.

1.2 Exciton states in semiconductors

1.2.1 Exciton in bulk semiconductors: three-dimensional case

An exciton is a bound electron-hole pair through the Coulomb interaction, and is generally created by the absorption of the photon of appropriate energy (in direct semiconductor). The energy levels $E_{n,K}$ of excitons are given by the simple hydrogenic model:

$$\begin{aligned} E_{n,K} &= E_g - \frac{\mu e^4}{32\pi^2 n^2 \hbar^2 \varepsilon_2^2 \varepsilon_0^2} + \frac{\hbar^2 K^2}{2(m_e^* + m_h^*)} \\ &= E_g - \frac{\hbar^2}{2\mu a_B^2} + \frac{\hbar^2 K^2}{2M} \\ &= E_g - E_b + E_K, \end{aligned} \tag{1.1}$$

Here, $K = k_e - k_h$ is the wave vector of exciton, E_g is the bulk energy gap at the center in the Brillourin zone, n (n=1, 2, 3,...) is the exciton quantum number; m_e^* and m_h^* are effective masses of the electron and hole, respectively; $\mu = \frac{m_e^* m_h^*}{m_e^* + m_h^*}$ is the reduced mass and $M = m_e^* + m_h^*$ is the translational mass of exciton; ε_2 is the dielectric constant of the semiconductor materials. The second term in Eq. (1.1) is the exciton binding energy $E_b = \frac{\hbar^2}{2\mu a_B^2}$; and the third term in Eq. (1.1) is the exciton

kinetic energy $E_K = \frac{\hbar^2 K^2}{2M}$ associated with the center-of-mass motion of the exciton. The exciton Bohr radius is given by

$$a_B = \frac{4\pi\varepsilon_0\varepsilon_2\hbar^2 n^2}{\mu e^2}, \qquad (1.2)$$

As a result of the interaction with the phonons, the exciton line shape is broadened and asymmetric at low temperature.

1.2.2 Exciton in low dimensional semiconductors

As stated above, the common feature of the low dimensional quantum structures is that they have the discrete electronic transitions which shift to higher energies with the decreasing of the size. In this part, we give a brief picture of the excitons in low dimensional semiconductors. The geometric illustrations of the different dimensional systems are shown in Fig. 1.1. Figure 1.2 shows the state density *N(E)* varies with

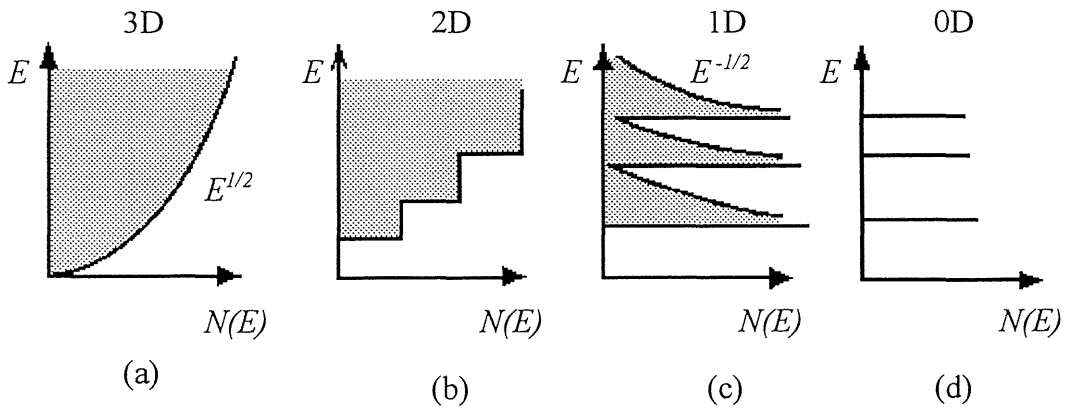

Fig. 1.2 State densities *N(E)* for ideal (a) 3D, (b) 2D, (c) 1D and (d) 0D systems.

the system dimensionality. From the three-dimensions to two-dimensions, one-dimension and zero-dimension, the state density changes from the continuous dependence of $N(E) \propto E^{1/2}$ (3D) to the step-like dependence (2D), the separated band dependence (1D) and the separated delta function dependence (0D). It means in the quantum dots, the oscillator strength is concentrated into just a few transitions.

Fig. 1.3 shows the exciton binding energies vary with sample size of the low dimensional CdS semiconductors. The ground state exciton binding energy E_b for the bulk CdS crystal is 28 meV, M=0.94 m_0, and ε_2=8.1; for the slab (2D), L_z =L is the thickness; for the wire (1D), L_x=L_y=L; for the quantum dot, L_x=L_y = L_z =L with L>3 a_B.

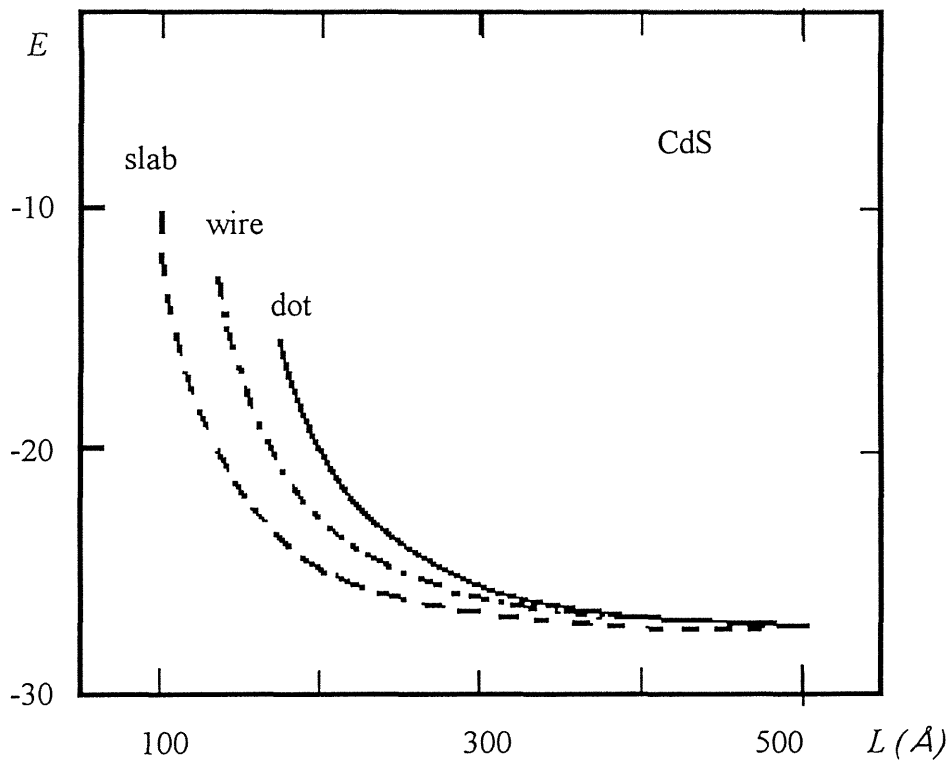

Fig. 1.3 Exciton energies for cubic CdS in the form of a slab, wire and quantum dot of size L. (After Ref. 26).

1.2.3 Exciton in semiconductor quantum dots

In case of the exciton, a confined electron and a confined hole coupled via the Coulomb interaction, in a spherical quantum dot, one has to deal with the Hamiltonian:

$$\mathrm{H} = -\frac{\hbar^2}{2m_e}\nabla_e^2 - \frac{\hbar^2}{2m_h}\nabla_h^2 - \frac{e^2}{\varepsilon|r_e - r_h|} + V_e(r_e) + V_h(r_h), \tag{1.3}$$

where m, r, and V represent mass, radius vector, and the potential, respectively.

The boundary conditions at the surface of the quantum dot are:

$$\psi_e(r) = \psi_h(r) = 0 \qquad when \qquad |r| \geq R. \tag{1.4}$$

The potential barrier is treated as:

$$V(r) = \begin{cases} 0 & (0 < r < R) \\ \infty & r \geq R \end{cases}, \tag{1.5}$$

it is illustrated in Fig. 1.4.

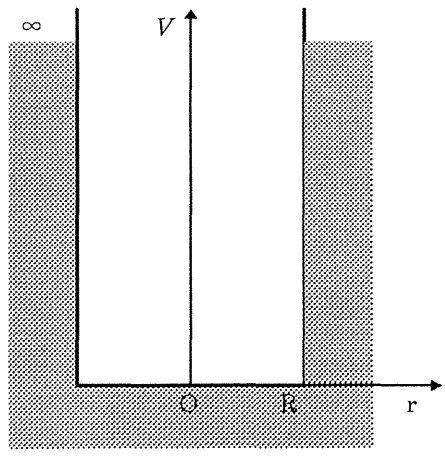

Fig. 1.4 The confinement potential barrier of a quantum dot.

For a Wannier exciton in a three-dimensional bulk material, the corresponding Hamiltonian without the confinement potentials V_e and V_h, the problem can be considered as the center-of-mass motion of the electron-hole pair. The binding energy of exciton is given by Eq. 1.1. However, it is difficult to get a common analytical expression of the binding energy of exciton in case of quantum dots. This is because that there is a strong symmetry breakdown in the quantum dots, as a result of the Coulomb interaction depends on the spatial coordinate between the electron and hole. The problem is analytically treated with two limiting conditions, i.e., the strong confinement situation ($R<<a_B$) and the weak confinement regime ($R>>a_B$).

In the limit $R >> a_B$, the electron-hole pair still can be considered as a quasiparticle of exciton while the translation freedom is confined with a small energy increment (the regime of the exciton confinement). The lowest energy is:

$$E = -E_{Ry}^{*} + \frac{\hbar^2 \pi^2}{2MR^2}, \tag{1.6}$$

where the higher-order terms decrease faster than R^{-2} [27].

In the opposite limit $R << a_B$, the electron and the hole should occupy primarily the individual lowest eigenstate of the zero-dimensional quantum well with relatively small spatial correlation (the regime of the individual particle confinement). The exciton energy is given as [28] :

$$E = \frac{\hbar^2 \pi^2}{2\mu R^2} - \frac{1.786 e^2}{\varepsilon R} - 0.248 E_{Ry}^{*}. \tag{1.7}$$

The third term comes from the exciton effect.

In Fig. 1.5, the numberical results of Kayanuma [27] and some experimental results on CuCl in NaCl crystal (○) [29], and CdS in glass (△) [30] are shown.

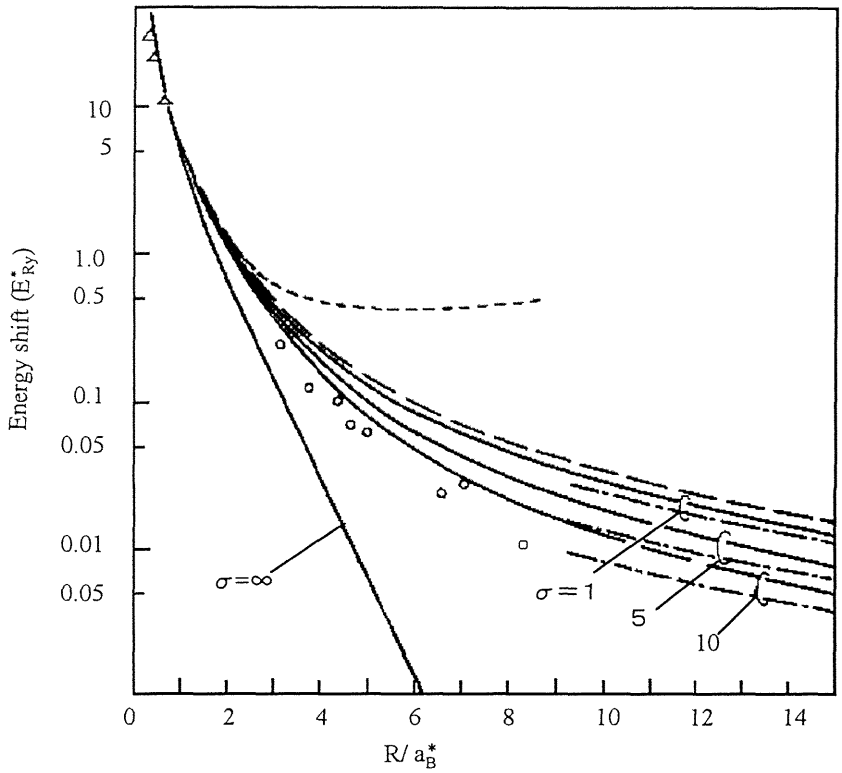

Fig. 1.5 The calculated energy shift of the ground state of exciton in the quantum dot (solid lines) with $\sigma \equiv m_h/m_e$ as a fixed parameter. The observed values of the luminescence peak in the CuCl quantum dot in NaCl (◯) and the absorption peak of CdS quantum dots in the silicate glass (△) are also plotted. After Ref. 27.

Recently, Richard et al. have considered the finite spin-obit splitting on the energy and wave-functions of valence band levels in some II-VI and III-V spherical semiconductor quantum dots [31]. Figure 1.6 shows their numerical calculated results on the valence band energy levels of CdS quantum dot and Figure 1.7 shows the calculated absorption spectrum of CdS quantum dots.

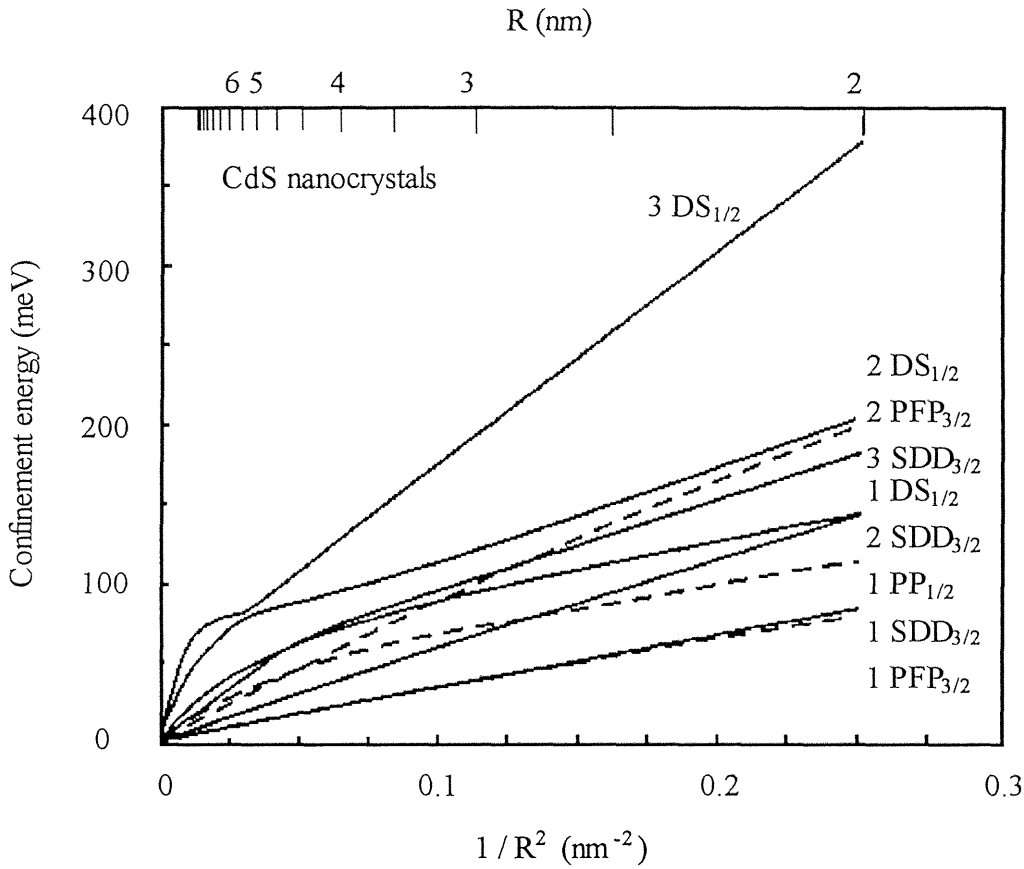

Fig. 1.6 Plot of the energies of some valence band levels in CdS quantum dots versus $1/R^2$ calculated by Richard [31]. Solid lines (dashed lines) represent levels for which interband transitions are allowed (forbidden) towards the 1Se lowest conduction band level. Here, the integer numbers, in the hole states, are the principal quantum numbers, the first and the second capital letters indicate the types of the orbit state (S, P, D,...) which are mixed, the last capital letters correspond to the component related to the spin-orbit split-off states, and the subscript indices correspond to the value of total angular momentum.

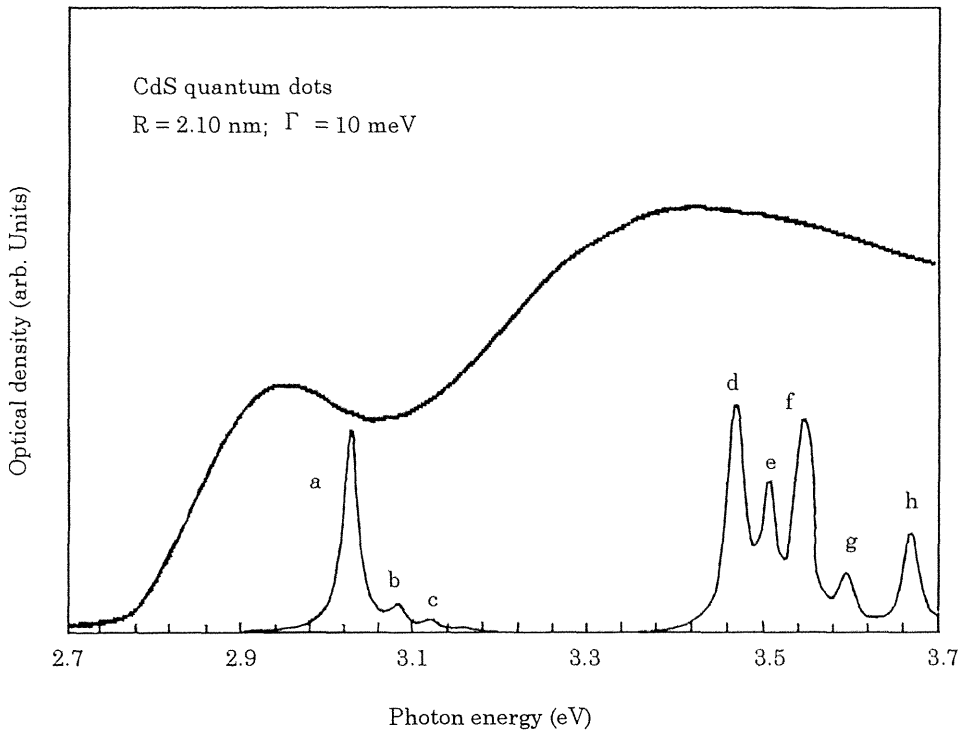

Fig. 1.7 The absorption spectrum of a crowd of CdS quantum dots of average radius 2.10 nm calculated by Richard [31]. The band gap of the system is 3.10 eV. The bottom and the top of the figure corresponding to two different size-dispersion functions (bottom: Dirac distribution; top: Gaussian distribution with σ =0.3 nm). Transitions labeled a-h correspond to 1Se-1SDD3/2, 1Se-2SDD3/2, 1Se-3SDD3/2, 1Pe-1PFP3/2, 1Pe-1PP1/2, 1Pe-1PFF5/2, 1Pe-2PFF5/2 and 1Pe-3PFF5/2, respectively. For valence band levels, the last letter corresponds to the L value of the spin-orbit split-off state involved.

The exciton oscillator strengths can also increase in the quantum dots. This is due to quantum confinement of both electrons and holes, and also because of the increased spatial overlap of electron and hole wave-functions. The exciton oscillator strength is expressed as :

$$f = \frac{2m_e^*}{\hbar^2}\Delta E|M|^2|U_{(0)}|^2, \qquad (1.8)$$

where $\triangle E$ is the transition energy, M is the transition dipole moment and $|U_{(0)}|^2$ is related to the probability of finding an electron and a hole on the same site (the overlap).

In the weak confinement regime ($R>>a_B$) , $|U_{(0)}|^2$ is independent of the size of quantum dot, and f is determined by the macroscopic transition dipole moment. The exciton oscillator strength of quantum dots, f_{QD}, increases linearly with the increase of quantum dot volume.

In the strong confinement regime ($R<<a_B$), $|U_{(0)}|^2$ increases with the decrease of the size of quantum dots. As a result, f_{QD} weakly depends on quantum dot size.

1.3 Properties of CdS crystal and quantum dots

1.3.1 Properties of bulk CdS crystal

The crystallographic properties of the $A^{II}B^{VI}$ semiconductors are remarkable, because their form is in either the wurtzite phase or zinc-blende phase. In the $A^{II}B^{VI}$ compounds, two valence electrons of the group II element and six electrons of the group VI element are distributed

according to the so-called s-p^3 orbital bonding configuration. In this picture, the highest-lying valence band is triply degenerate (in the absence of spin-orbit splitting), and the states at the center of the Brillourin zone are bonding combinations of p-like functions. The lowest conduction band is s-like.

The introduction of spin-orbit interaction alters the bands, principally, by splitting certain degeneracies. Figure 1.8 gives the detail of the band structure around k=0 of zinc-blende structure and wurtzite structure, respectively.

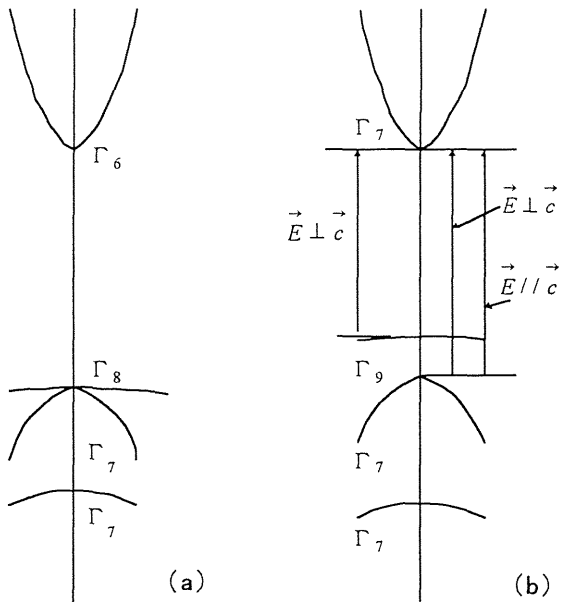

Fig. 1.8 The band structure around k=0 of (a) zinc blend structure and (b) wurtzite structure. (b) also shows the selection rule for optical transitions near the band edge for wurtzite structure.

Table 1.1 Basic physical properties of some II-VI semiconductor*

Semiconductor	Crystal structure+	Lattice constant (Å) ao	co	Eg (eV) 4 K	300K	Dielectric constant ε_2	effective mass (m_0) m_e^*	m_h^*	Phonon Energy (cm^{-1}) LO	TO	Exciton binding energy E_b (meV)	Exciton Bohr radius a_B(Å)
CdS	WZ	4.1368	6.7163	2.58	2.422	8.6	0.171(⊥) 0.153 (//)	0.7(⊥) 5 (//)	300	282	27	30
CdSe	WZ	4.30	7.02	1.82	1.75	9.4	0.112(⊥)	0.45(⊥) 0.62 (100)	218	186	14-16	54
ZnSe	ZB	5.668		2.82	2.67	8.8	0.17	0.7	208	212	18-20	38 (WZ)

---

* The physical parameters present here are summarized on basis of following source references:

1. A. D. Yoffe, *Adv. Phys.* 42, 173 (1994).
2. S. S. Mitra, *Phys. Rev.* 132, 986 (1963).
3. M. Balkanski and J. M. Besson, *J. Appl. Phys.* 32, 22292 (1961).

\+ "WZ" and "ZB" indicate wurtzite and zinc-blende, respectively.

The lattice structures of semiconductor CdS and CdSe are of wurtzite type, and the point group of them is C_{6v} symmetry. The lattice structure of semiconductor ZnSe is of zinc-blende type, and its point group is T_d symmetry.

Some fundamental physical properties of CdS, CdSe and ZnSe crystal are shown in Table 1.1.

1.3.2 Properties of CdS quantum dot

Although Ⅱ-Ⅵ semiconductor quantum dots embedded in either the glass or in the polymer matrix are the most widely studied quasi-zero-dimensional structures, it is difficult to give a satisfied description on the optical properties of them. There is a controversy in the observations in the photoluminescence and the photoinduced spectral hole burning. The observations depend on the samples being used, and depend on the surface properties of the sample. Obviously, these issues need further investigations. We will describe the subjects further in the later parts.

1.4 Diluted magnetic semiconductor quantum dots

1.4.1 Properties of bulk diluted magnetic semiconductor

The diluted magnetic semiconductor (DMS) or semimagnetic semiconductor is that the semiconductor with a fraction of its constituent ions is replaced by some species of magnetic ions (i. e., ions bearing a net magnetic moment, such as the transition metal cations: Mn^{2+}, Fe^{2+}, or the rare earth metal cation: Eu^{2+}). So far, majority of DMS studies were done with the bulk $A^{\mathrm{II}}_{1-x}Mn_xB^{\mathrm{VI}}$ mixed crystals and the low dimensional

quantum structures on basis of $A^{II}_{1-x}Mn_xB^{VI}$. The reasons may be:

① Mn^{2+} can be incorporated in sizable amounts in the $A^{II}B^{VI}$ host without affecting substantially the crystallographic quality of the resulting material (e. g., up to nearly 80% of Mn can be added in CdTe, and nearly 50% in case of CdS, see Fig. 1.9).

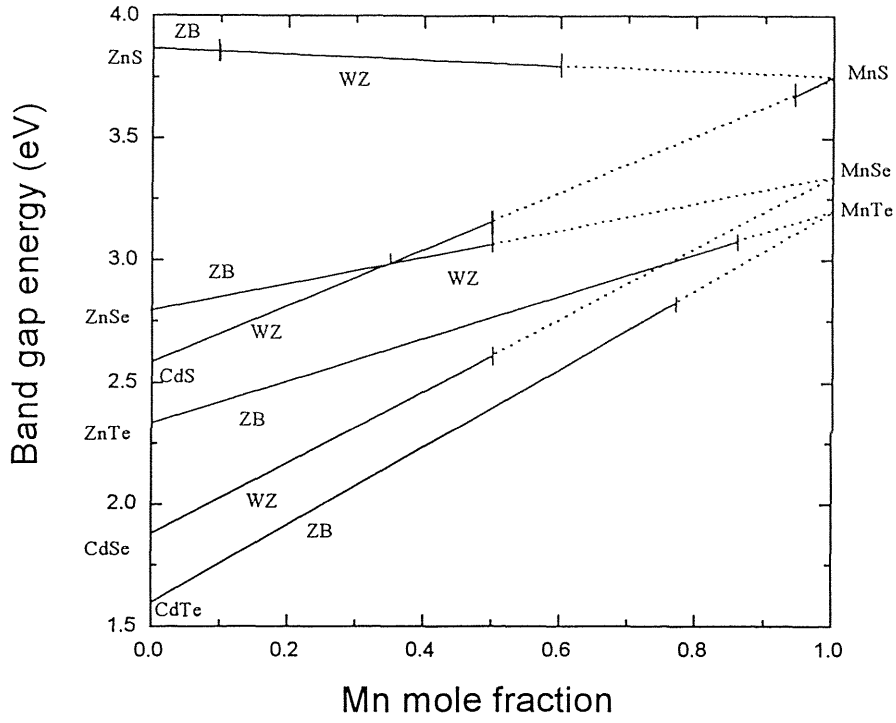

Fig. 1.9 A summary of the energy gap (E_g) as a function of the Mn mole fraction(x); for the (Zn, Mn) and (Cd, Mn) chalcogenides at low temperature (~4 K) in linear approximation. The solid lines indicate ranges of the molar fraction x for which homogeneous crystal phases are formed. "WZ" and "ZB" indicate wurtzite and zinc-blende, respectively. Dashed lines: extrapolations into the miscibility gap.

② Mn^{+2} possesses a relatively large magnetic moment (S = 5/2), characteristic of a half-filled d shell (from this point of view, Eu^{+2} with S=7/2 might be even more attractive);

③ Mn^{+2} is electrically neutral in $A^{II}B^{VI}$ hosts, i.e., it constitutes neither an accepting nor a donating center.

There are three aspects of DMS properties that make these alloys interesting.

① The band gap of the material can be varied by changing the Mn^{+2} mole fraction in the crystal. Similarly, the lattice parameters can be tuned by varying the composition (Fig. 1.9).

② The magnetic properties of DMS, including paramagnetic, spin-glass and antiferromagnetic properties, are studied. It is possible to study all these magnetic features systematically as a function of the concentration of Mn^{+2}.

③ The interaction between the localized magnetic moments of Mn^{+2} and the conduction band electrons, and valence band holes (which are referred as the s, p-d interaction) results in a series of unique features. The best known features are the huge Faraday rotation of the visible and near-infrared light and the giant negative magnetoresistance in DMS. These impressive features have their common origin in the s, p-d exchange interaction.

At very low concentration of Mn (typically below 1 atomic percent), the influence of Mn on the band structure can be disregarded. When larger mole fractions of Mn (of a few atomic percent or more) are alloyed with $A^{II}B^{VI}$ host material, the situation is drastically altered. The changes of these kinds of DMS' band gaps with the Mn concentration x

are shown in Fig. 1.9.

The introduction of Mn not only changes the band structure of the host $A^{II}B^{VI}$ semiconductor, but also introduces new optical transition levels. These include prominent absorption and emission features, which can be correlated with the expected splitting of Mn multiplets in a crystalline field.

Significant understanding of this aspect of DMS can be obtained by considering an isolated Mn ion in an $A^{II}B^{VI}$ lattice. A free Mn atom has the $3d^5 4s^2$ ground state configuration for the outermost shells. Its ground state is ^6S and the excited states are ^4G, ^4P, ^4D, ^4F, etc., in order of increasing energy. When an Mn atom is put into a DMS, it substitutes for the cation. Two 4s electrons form the bonds with the surrounding ions, and five 3d electrons interact strongly with the electrical potential of the nearest neighbor anions. In the crystal field, the states of free Mn atom are split. In analyzing experimental data and making assignments concerning absorption and emission, the diagrams presented by Tanabe and Sugano [32] are very useful. In these diagrams the variations of energy level are plotted against crystal field strength in the octahedral symmetry.

Details of Mn^{2+} optical transitions in $A^{II}B^{VI}$ semiconductors have been the subject of intense investigation for many years, but the results were predominantly confined to samples with Mn in extreme dilution. In this regime, details of vibrational interactions, Jahn-Teller effects, and other phenomena requiring high resolution spectroscopy could be studied because of the rich structures of the spectrum. Such structures disappear rapidly with $x \geq 0.01$, and only broad excitation and emission

features remain as the Mn concentration is further increased.

The Mn-related absorption/excitation bands seen in various DMS, the corresponding intra-ion transitions, and in several selected cases, also crystal field parameters employed in the analysis of the data are listed in Table 1.2. In all $A^{II}_{1-x}Mn_xB^{IV}$ DMS where E_g exceeds 2.2 eV, a broad (FWHM $\approx$ 0.1eV) photoluminescence band is seen in the yellow region of the spectrum. This transition is generally accepted as the $^4T_1(^4G) \rightarrow {}^6A_1(^6S)$ transition, and is the emission associated with the excitation bands listed in Table 1.2.

Table 1.2 A summary of Mn^{2+} absorption/excitation band maxims (in eV) in the (Zn, Mn) and (Cd, Mn) chalcogenides DMS alloys

DMS Alloy	$^6A_1 \rightarrow {}^4T_1$	$^6A_1 \rightarrow {}^4T_2$	$^6A_1 \rightarrow {}^4A_1, {}^4E$	other	x	Reference
$Cd_{1-x}Mn_xTe$	~2.2				0.4≦x≦0.7	33, 34
	~2.2	~2.5			0.4≦x≦0.7	35
		~2.43*	~2.63*		0.7	36, 37
		~2.4*	~2.6*		0.7	38
$Cd_{1-x}Mn_xSe$	~2.3 (Threshold)				~0.48	39
$Cd_{1-x}Mn_xS$	2.43	2.58	2.72		~0.4	40
$Zn_{1-x}Mn_xTe$	~2.3	~2.36			~0.1	41
	~2.3	~2.38	~2.576		~0.5	41
	~2.33	~2.40	~2.605	~2.745	~0.6	41
	B (cm-1)	C (cm-1)	Dq (cm-1)			
	720	2664	743 (T_d), 330 (O_h)		~0.1	41
	713	1638	750 (T_d), 330 (O_h)		~0.5	41
	713	2637	913 (T_d), 400 (O_h)		~0.6	41
$Zn_{1-x}Mn_xSe$	2.34	2.48	2.655		0.001	42
	2.38	2.57	2.68		0.23	43
	2.4	2.5	2.70	2.9	0.35	43
	2.42	2.54	2.70	2.93	0.5	43
	B (cm-1)	C (cm-1)	Dq (cm-1)			
	750	2730	836 (T_d), 372 (O_h)		0.23	43
	749	2772	830 (T_d), 369 (O_h)		0.35	43
	751	2782	795 (T_d), 353 (O_h)		0.5	43
$Zn_{1-x}Mn_xS$	2.22	2.44	2.635	2.815 3.13	<0.01	44
	2.35	2.53	2.69	2.96, 3.13	0.216	

* Assignments ambiguous because of broadening and overlapping of bands.

In DMS, a variety of remarkable magneto-optical properties have been observed due to the exchange interaction of the band electrons with the magnetic ions. The exchange interaction of the exciton with the Mn^{2+} ions is given by

$$E_{exch} = N_0(\beta - \alpha)x\langle S_z \rangle, \tag{1.9}$$

where N_0 is the number of unit cells per unit volume, α and β are the exchange parameters of the interaction of electrons and holes with the Mn^{2+} ions, respectively, x is the mole fraction of Mn^{2+} and $\langle S_z \rangle$ is the z component of Mn^{2+} spins. In the presence of an external magnetic field, this exchange interaction causes a large spin splitting described by a giant effective g factor given by

$$g_{eff} = g_0 + E_{exch} / \mu_B H, \tag{1.10}$$

where g_0 is the g factor of the excitons as determined by the energy band parameters, μ_B is the Bohr magneton, and H is the magnetic field. The exchange interaction induces a giant g factor for the excitons and in their Zeeman effect under magnetic field appears as the marked energy shifts in the absorption, reflectivity, and photoluminescence spectra of the exciton. Remarkable enhancement of the exciton luminescence intensity with increasing magnetic polaron effect in the exciton states has been intensively studied in the quantum wells as well as in the bulk crystals.

1.4.2 Properties of diluted magnetic semiconductor quantum dots

As above mentioned, wide band gap $A^{II}_{1-x}Mn_xB^{IV}$ semiconductor mixed crystals are typical and the most extensively studied DMS. Their physical properties are characterized by the combination of the

properties of nonmagnetic semiconductor mixed crystals with the special properties caused by the half-filled 3d-shell of the Mn^{2+} cations. They have attracted continuously growing interests from both basic and application sides. The further studies are stimulated by the successful preparation of DMS quantum structures. The DMS properties bring new physical aspects into the already rich and exciting phenomena of low dimensional quantum structures.

Since the first successful preparation of DMS superlattices and multi-quantum well structures in 1984 on the basis of (Cd,Mn)Te [45-46], many works have been done on DMS nanostructures. The magneto-optical properties are explained by the s,p-d exchange interaction [47]. The magnetic phase transitions in quantum well structures were observed due to the antiferromagnetic interaction between neighboring Mn ions [48].

The DMS quantum dots are interesting since both the quantum size effect and the quantum confined exchange effect arise. In the quantum dots, the electronic states are significantly modified from those of the bulk materials. The magneto-optical properties due to strong sp-d exchange interaction between the band carriers and Mn^{2+} ions have been extensively studied in bulk and two dimensional DMS materials. A similar situation is expected in an optically excited DMS quantum dot.

Wang et al. reported the first experimental investigation of DMS quantum dots in 1991 [49]. In their case, $Zn_{0.93}Mn_{0.07}S$ crystallites of average diameter 25Å were grown in a glass matrix. The observed photoluminescence peak at 2.12 eV corresponds to the well-known Mn^{2+} internal emission. They also measured the static magnetic susceptibility from 2.3 K to 314 K; the data fit the Curie-Weiss law with

a negligibly small Θ value, suggesting a smaller contribution of the antiferromagnetic Mn-Mn interaction in the quantum dot than in the bulk. More recently, Bhargava *et al.* fabricated coated Mn-doped ZnS particles of diameter varying from 35 to 75 Å [50]. They focused on the characteristics of the Mn^{2+} luminescence: a high luminescence efficiency and a dramatically short decay time were observed. However, the mechanism of these novel optical properties is not well known. Moreover, some observations showed different results [51-52].

In some narrow band gap $A^{II}_{1-x}Mn_xB^{VI}$ semiconductor quantum dots, like $Cd_{1-x}Mn_xTe$ and $Cd_{1-x}Mn_xSe$, the exciton luminescence shows the excitonic magnetic polaron (EMP) effect in the quantum dots [53]. Marked decrease of the exciton lifetime is observed with increasing the magnetic field.

1.5 Applications

One of the most important reasons why the research of quantum dots has been progressing greatly during the passed decade is the strong technological interest, because the quasi-zero-dimensional systems exhibit new quantum phenomena and have potential applications for becoming novel devices. There are several active research fields of the applications of quantum dot.

The saturation of optical absorption which is easily to be observed in the semiconductor doped glasses and polymers may be used to develop different devices for modulating and controlling optical signals by light [54]. There are two main advantages of these materials compared to the bulk semiconductors and organic dyes. The first is a very wide

tuning range of the nonlinear absorption spectrum. The second is a very high contrast provided by semiconductor doped glasses as an absorption saturator.

Using quantum dot system as a gain medium to produce the quantum dot laser is another active research field in the application study of quantum dots [55-56].

Similar to the bulk and two-dimensional semiconductors, quantum dots have been demonstrated that they can be used to be photodiode and electro-luminescence devices. However, the research on this subject is at early stage, because the reported efficiencies are extremely low [57-58].

The persistent spectral hole burning in the quantum dots, a recent found novel phenomenon in quantum dots by the group that author belongs to, has a potential application as a photo-recording and reading memory medium [59]. And the investigation on the persistent spectral hole burning in the quantum dots embedded in polymer matrix is a part of this research.

1.6 Objective of this work

The purpose of this research work is to explore the novel optical properties originating from the quantum dot structures and study their mechanisms, thereby open up a new regime in the material science of potential applications.

In particularly, in this research work we have systematically

investigated the optical properties of CdS quantum dots by means of a variety of spectroscopy measurements. We investigated the persistent spectral hole burning in quantum dots embedded in polymer matrix; and the photoluminescence of CdS quantum dots and CdS:Mn quantum dots in zero external field.

References

[1] For the reviews, see Ⅰ. L. E. Brus, *Appl. Phys.* A 53, 465 (1991). Ⅱ. A. D. Yoffe, *Adv. Phys.* 42, 173 (1993), and references therein. The concepts of quantum dots even can be seen in some modern text on solid state physics.

[2] N. Nogami and A. Nakamura, *Phys. Chem. Glasses* 34, 109 (1993).

[3] U. Woggon, S. V. Bogdanov, O. Wind and V. Sperling, *J. Crystal Growth* 138, 976-980 (1994).

[4] G. Li and M. Nogami, *J. Appl. Phys.* 75, 4276. (1994).

[5] D. J. Norris and M. G. Bawendi, *J. Chem. Phys.* 103, 5260 (1995).

[6] J. Qi and Y. Masumoto, *Solid State Commun.* 99 467 (1996).

[7] M. C. Klein, F. Hache, D. Ricard and C. Flytzanis, *Phys. Rev.* B 42, 11123, (1990).

[8] M. G. Bawendi, W. L. Wilson, L. Rothberg, P. J. Carroll, T. M. Jedju, M. L. Steigerwald and L. E. Brus, *Phys. Rev. Lett.* 65, 1623 (1990).

[9] D. J. Norris, A. Sacra, C. B. Murray and M. G. Bawendi, *Phys. Rev. Lett.* 72, 2612 (1994).

[10] M. A. Hines and P. Guyot-Sionnest, *J. Phys. Chem.* 100, 468-471 (1996).

[11] A. Roy and A. K. Sood, *Solid State Commun.* 97, 97-102 (1996).

[12] V. Esch, B. Fluegel, G. Khitrova, H. M. Gibbs, Xu Jiajin, K. Kang, S. W. Koch, L. C. Liu and S. H. Risbud, *Phys. Rev.* B 42, 7450 (1990).

[13] T. Rajh, O. I. Mícíc and A. J. Nozik, *J. Phys. Chem.* 97, 11999 (1993).

[14] P. Lefebvre, T. Richard, J. Allègre, H. Mathieu, A. Pradel, J. L. Marc, L. Boudes, W. Granier and M. Ribes, *Superlattices Microstruc.* 15, 447 (1994).

[15] S. Yano, T. Goto, and T. Itoh, *J. Appl. Phys.* 79 (11), 8216-8221 (1996).

[16] Y. Masumoto, S. Okamoto and S. Katayanagi, *Phys. Rev.* B 50, 18658 (1994).

[17] R. L. Wells, C. G. Pitt, A. T. Mcphail, A. P. Purdy, S. Shafieezad and R. B. Hallock, *Chemistry of Materials* 1, 4-6 (1989).

[18] M. A. Olshavsky, A. N. Goldstein, and A. P. Alivisatos, *J. Am. Chem. Soc.* 112, 9438-9439 (1990).

[19] O. I. Micic, J. R. Sprague, C. J. Curtis, K. M. Jones, J. L. Machol, A. J. Nozik, H. Giessen, B. Fluegel, G. Mohs and N. Peyghambarian, *J. Phys. Chem.*, 99, 7754-7759 (1995).

[20] A. A. Guzelian, J. E. B. Katari, A. V. Kadavanich, U. Banin, K. Hamad, E. Juban, A. P. Alivisatos, R. H. Wolters, C. C. Arnold and J. R. Heath, *J. Phys. Chem.*, 100, 7212-7219 (1996).

[21] A. A. Guzelian, U. Banin, A. V. Kadavanich, X, Peng, and A. P. Alivisatos, *Appl. Phys. Lett.*, 69, 1432-1434 (1996).

[22] Y. Kanemitsu, *Phys. Rep.* 263, 1-91 (1995).

[23] Al. L. Efros and A. L. Efros, *Soviet Phys. - Semicond.* 16 , 772 (1982).

[24] A. I. Ekimov and A. A. Onushenko, *Soviet Phys. - J. Exper. Theor. Phys. Letters* 40, 1137 (1984).

[25] R. Rosetti, R. Hull, J. L. Ellison and L. E. Brus, *J. Chem. Phys.* 80, 4464 (1984).

[26] D' Andrea and Del Sole, *Solid State Commun.* 74, 1121 (1990).

[27] Y. Kayanuma, *Phys. Rev.* B 38, 9797, (1988).

[28] L. E. Brus, *J. Chem. Phys.* 80, 4403 (1984); ibid., 90, 2555 (1986).

[29] T. Itoh, Y. Iwabuchi and M. Kataoka, *Phys. stat. sol.* b 145, 567 (1988).

[30] A. I. Ekimov, Al. L. Efros and A. A. Onushenko, *Solid State Commun.* 56, 921 (1985).

[31] T. Richard, P. Lefebvre, H. Mathieu, and J. Allègre, *Phys. Rew. B* 53, 7287-7298 (1996).

[32] Y. Tanabe and S. Sugano, *J. Phys. Soc. Japan* 9, 753-779 (1954).

[33] R. Y. Tao, M. M. Moriwaki, W. M. Becker, and R. R. Galazka, *J. Appl. Phys.* 53, 3772 (1982).

[34] Y. R. Lee, and A. K. Ramdas, *Solid State Commun.* 51, 861 (1984).

[35] M. M. Moriwaki, W. M. Becker, W. Gebhardt, and R. R. Galazka, *Phys. Rev. B.* 26, 3165 (1982).

[36] G. Rebmann, C. Rigaux, G. Bastard, M. Menant, R. Triboulet, and W.

Giriat, *Physica* 117B & 118B, 452 (1983).

[37] J. Diouri, J. P. Lascaray, and M. El Amrani, *Phys. Rev. B.* 31, 7995 (1985).

[38] J. P. Lascaray, J. Diouri, M. El Amrani, and D. Coquillat, *Solid State Commun.* 47, 709 (1983).

[39] J. E. Morales, W. M. Becker, and U. Debska, *Phys. Rev. B.* 32, 5202 (1985).

[40] M. Ikeda, K. Itoh and H. Sato, *J. Phys. Soc. Japan.* 25, 455 (1968).

[41] J. E. Morales Toro, W. M. Becker, B. I. Wang, U. Debska, and J. W. Richardson, *Solid State Commun.* 52, 41 (1984).

[42] D. W. Langer, and D. W. Richter, *Phys. Rev.* 146, 554 (1966).

[43] J. E. Morales Toro, *Ph. D. Thesis,* (1985). Purdue University, unpublished.

[44] D. Langer, and S. Ibuki, *Phys. Rev.* A 138, 809 (1965).

[45] R. N. Bicknell, R. W. Yanka, N. C. Giles-Taylor, D. K. Blanks, E. L. Buchland, J. F. Schetzina, *Appl. Phys. Lett.* 45, 92 (1984).

[46] L. A. Kolodziejski, T. C. Bonsett, R. L. Gunshor, S. Datta, R. B. Bylsma, W. M. Becker, N. Otsuka, *Appl. Phys. Lett.* 45, 92 (1984).

[47] X. C. Zhang, S. K. Chang, A. V. Nurmikko, L. A. Kolodziejski, R. L. Gunshor, S. Datta, *J. Lumin.* 34, 89 (1985).

[48] L. L. Zhang, *Superlattices and Microstructures* 6, 39 (1989).

[49] Y. Wang, N. Herron, K. Moller and T. Bein, *Solid State Commun.* 77 (1), 33-8 (1991).

[50] R. N. Bhargava, D. Gallagher, X. Hong, A. Nurmikko, *Phys. Rev. Lett.* 72 (3), 416-19 (1994).

[51] M. A. Chamarro, V. Voliotis, R. Grousson, P. Lavallard, T. Gacoin, G. Counio, J. P. Boilot and R. Cases, *J. Crystal Growth* 159, 853 (1996).

[52] T. Yoshiue, H. Iwata, M. Kobayashi, Y. Kobayashi, S. Endo, *Proc. 2nd Asia Sym. Cond. Mat. Photophys.* 365 (Nara, 1996).

[53] K. Yanata and Y. Oka, *Superlattices Microstruct.* 15 (3), 233-6 (1994).

[54] U. Woggon and S. V. Gaponenko, *Phys. stat. sol.* b 189, 285 (1985).

[55] Y. Z. Hu, H. Gieβen, N. Peyghambarian, and S. W. Koch, *Phys. Rew. B* 53, 4814-4822 (1996).

[56] Y. Masumoto, T. Kawamura and K. Era, *Appl. Phys. Lett.* **62**, 225 (1993).

[57] B. O. Dabbousi, M. G. Bawendi, O. Onitsuka and M. F. Rubner, *Appl. Phys. Lett.* **66** (11), 1316-1318 (1995).

[58] V. L. Colvin, M. C. Schlamp and A. P. Alivisatos, *Nature* **370**, 354 (1994).

[59] K. Naoe, L. G. Zimin, Y. Masumoto, *Phys. Rev.* B **50**, 18200 (1994).

2 Samples

2.1 Introduction

A variety of techniques have been used in the preparation of quasi-zero-dimensional semiconductors. The quasi-zero-dimensional semiconductors may be in the form of powders, dispersed in inorganic glasses or organic polymers, and in the crystalline such as GaAs, NaCl, and so on. In Section 2, we simply review the currently used methods in the fabrications of quantum dots. We mainly focus on the synthesis of the compound semiconductor quantum dots embedded in the polymer matrixes, since they are the commonest methods used by researchers in preparing CuCl, CuBr, and various II-VI, III-V semiconductor quantum dots. They can give near monodispersed quantum dots in a matrix and new hybrid nanometer structures. The fabrications of silicon related single element semiconductor quantum dots are not included here, as there are many related reviews [1]. Then, we describe our method of synthesis II-VI semiconductor quantum dots and Mn doped II-VI semiconductor quantum dots embedded in polyvinyl alcohol and the characterization of these quantum dots by small angle X-ray scattering measurements.

2.1.1 Quantum dots in a polymer matrix

Presently, a number of techniques are available in preparing II-VI, III-V semiconductor quantum dots in an organic matrix. These techniques use the methods of organometallic reactions and polymer chemistry at near room temperature [2-17].

The basic features of the method are:

① The relatively low preparation temperature (usually not more than 200℃) is favorable to minimize the number of lattice defects.

② The possibility to cap the crystallite surface by organic groups, inorganic groups, and molecules.

③ It is possible to get isolated quantum dots or to disperse them in a thin film.

④ An extremely narrow size distribution of the quantum dots can be obtained. For example, the well-developed method of fabrication of CdSe can lead to nearly monodisperse size dispersion less than 5% and well-defined crystalline [7].

The size of quantum dots can be controlled by the temperature, the mixing rate of the reagents, as well as by the concentration of the stabilizer [4-5]. To merge the nanocrystallites into the inverse micelles [5], liposome vesicles [18] and zeolites [19], etc. also can lead the controlled size of quantum dots.

The high surface-to-volume ratio of small quantum dots suggests that the surface properties should have significant affections on their structure and optical properties. While surfaces capped by various organic or inorganic layers appear to influence only mildly the absorption characteristics, it is well-known that the emission efficiency, spectrum, and time evolution are strongly affected by the surface. This is generally understood as the presence of surface trap states arising from surface nonstoichiometry, unsaturated bonds, etc. These surface states trap electrons or holes and degrade the optical properties of the materials. The control of the surface is a key to prepare high quantum yield quantum dots. Both the organic materials or inorganic materials

have been used for surface control. The surface chemical control process is called surface passivation or capping. It is made through bonding the surface atoms to another material of a much large band gap, eliminating all of the energy levels inside the gap. The ideal termination naturally removes the reconstructions, strains, and produces an abrupt jump in the chemical potential for electrons and holes at the interface.

It is possible to use a polymer material as both the stabilizer and matrix [15, 20]. Polyvinyl alcohol (PVA) and polymethylmethacrylate (PMMA) are known as well-suited matrix materials. The obtained quantum dots in these matrixes have clearly resolved absorption bands and intense luminescence. The film can easily be made very thin with the thickness of 10 μm or even less. A method developed by Bawendi et al. [6] using the tri-n-octylphosphine (TOP), tri-n-octylphosphine oxide (TOPO) as stabilizer and capping materials, can make CdSe quantum dots with the narrowest dispersion of size (known as the best quantum dots up to now) and a high quantum yield (~0.9 at 10 K). This kind of method seems very suited for making nanostructures in the polymer matrix and has been applied to make other II-VI [17, 21], III-V [22-24] nanometer semiconductors, and new hybrid nanometer semiconductors [25, 26]. Organically capped quantum dots can have a quantum yield of ~10% at room temperature reaching nearly 100% at low temperature [6-7], but at the expense of a very long (microsecond) fluorescence lifetime. It means these quantum dots do not have a perfectly passivated surface. They also exhibit some red shifted luminescence and complex decay of the excited state [8]. Obviously, the organic passivation needs further improvements on it.

Inorganic capping is another alternative way. Nanometer semiconductors capped by inorganic layer have been studied by several groups. The systems studied are (CdS)$Cd(OH)_2$ [16, 27], (CdSe)ZnS [17], (CdSe)ZnSe [28], ((CdS)HgS)$Cd(OH)_2$ [25-26], (ZnS)MnS [29], (CdS)MnS [30] and (CdS)Ag [31]. Proper choice of the cap material can lead to enhancement of charge transfer or improved luminescence [17, 30]. The ZnS-capped CdSe quantum dot exhibits strong band edge luminescence with a 50% quantum yield at room temperature [17]. It is the highest emission quantum yield of quantum dots so far reported at room temperature. Using highly luminescent samples, the single quantum dot luminescence spectra have been studied recently [32-33].

Besides the above organometallic chemical methods, there is a special physical method to prepare CuCl, CuBr quantum dots in the polymer matrix by using the polymer solution. The mixture of CuCl organic solution and polymer solution is dried under a low vacuum till stick film was obtained, then the quantum dots are formed by annealing the film in the temperature region of 85-200℃ [34].

2.1.2 Other techniques

There are several other ways to make quasi-zero-dimensional semiconductors.

The growth method of semiconductor quantum dots in the glass host is widely used for II-VI [35-37], and I-VII compounds [38]. This method is based on the commercial technologies developed for manufacturing color cutoff filters and photochromic glasses, which are known over decades (or even over centuries in the sense of color glasses). The

semiconductor quantum dots surrounded by amorphous glass and with mean size between one and several ten nanometers can be obtained by using this method. Most widely used matrixes are silicate, borosilcate and germanium oxide glasses with the absorption onset near 4 eV. The optical transparency of the glass host allows optical spectroscopy of the semiconductor inclusions over the whole visible spectral range.

For nanometer cuprous halide semiconductors, a successful example is embedding them into the sodium halides (potassium halides) crystals. Many works have demonstrated that the porous materials as zerolites [19], sol-gel glasses [39-41], or other porous glasses can be used as the host matrixes of nanometer semiconductor.

As well used for fabrications of the quantum well structures, the molecular beam epitaxy (MBE) and metalorganic chemical vapor deposition (MOCVD) techniques, are no doubt useful in fabrication of quantum dot array. The research works are performed mainly on the III-V based structures [42-43].

Rf sputtering method is also used in synthesis of the quantum dots as CuCl, CdTe:Mn [44-45], etc.

2.2 Experiments

In this work, we have fabricated CdS, CdSe, ZnSe quantum dots, and the Mn^{2+} doped corresponding dots, CdS:Mn, CdSe:Mn, ZnSe:Mn quantum dots, and investigated their optical properties. In this part, we present our method of preparation of CdS, CdSe, ZnSe and CdS:Mn, CdSe:Mn, ZnSe:Mn quantum dots embedded in polyvinyl alcohol and the

characterization of the quantum dots by small angle X-ray scattering measurements.

2.2.1 Fabrication of CdS quantum dots

In this work, we have made the following considerations in preparing the quantum dot samples.

① The sample should have a narrow size dispersion and thus have a sharp absorption edge;

② The sample should be stable enough during a serious optical measurements. This means the sample does not show obvious changes in absorption and luminescence;

③ The sample should be easily handled both at room temperature or liquid helium temperature.

We used the method of organometallic reactions and polymer chemistry at near room temperature to synthesize the nanometer semiconductors. We chose polyvinyl alcohol (PVA) polymer as the host matrix. As stated in the former part of this section, PVA polymer may act as both the stabilizer and matrix, simultaneously. It is easy to make the film very thin with the thickness of 10 μm or even less. The obtained quantum dots have clearly resolved absorption bands and intense luminescence.

As the stabilizing agents, PVA, 2-mercaptoethanol (RSH) and NaOH were used. The nanostructure size can be controlled by the concentration of RSH. The reason why we add NaOH into the solution to preparing the quantum dots under high pH conditions is that $Cd(OH)_2$ as capping materials can weaken the deep trap luminescence centers

and that this procedure results in relatively larger quantum yield of luminescence [32].

We used two different methods to prepare quantum dots. The reagents: cadmium chloride ($CdCl_2$), sodium sulfide ($NaS \cdot 9H_2O$), sodium selenide (Na_2Se), zinc chloride ($ZnCl_2$), 2-mercaptoethanol (RSH), and polyvinyl alcohol (They were obtained from Kanto Chem., Furuuchi Chem. and Wako Chem. The degree of polymerization of PVA = 2000) were used without further purification. The samples were prepared by the following procedure:

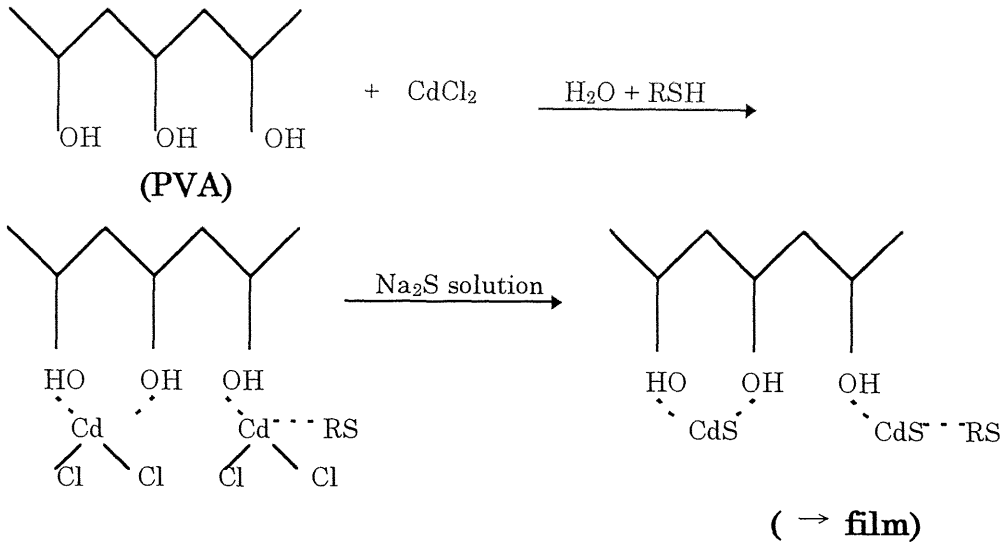

+ NaCl (soluble in water) .

The first method, so-called the casting method, is described as follows. Aqueous solution of $CdCl_2$ (10mM/1ml) was mixed with an aqueous solution of PVA (1mg/10ml). The adequate amount of RSH was added to the mixed solution for the control of the size of quantum dots, because $CdCl_2$ adsorbed by RSH was protected from forming CdS. Next, the fresh Na_2S/NaOH aqueous solution was added to the mixture in the dark. The quantity of S^{2-} controlled the ratio of Cd^{2+}/ S^{2-}. The mixture was

stirred by a magnetic stirrer throughout all these processes. The resultant solution was dried in a nitrogen atmosphere at 40℃ for more than 6 hours and then was cast onto a cover glass plate. The precursor film was dried further at 40 mmHg for one day.

Another method is an improved one which can easily control the size of quantum dots and the thin film. First, 0.01mM $CdCl_2$ was dissolved and the adequate amount of RSH was added into the aqueous solution of PVA (1mg/10ml). After being stirred sufficiently, the resultant solution was cast onto the cover glass plate. Then it was dried in the vacuum at 70℃ for more than 4 hours. Next, the film was put into the solution of S^{2-} (30g Na_2S and 5ml of 2N NaOH solution dissolved into 100ml H_2O) at 70℃. After several minutes the film was taken out and washed with the distilled water, and dried in vacuum at 70℃ for more than 6 hours. The films about 20-80 μ m thick were optically transparent, colorless, and can be easy to be handled, e.g., be cut, bent and taken off from the glass base.

CdSe and ZnSe quantum dots are fabricated by the similar methods as described above.

2.2.2 Fabrication of CdS:Mn quantum dots

The DMS quantum dots can be prepared by a variety of methods, such as MBE, MOCVD, rf-sputtering [45-46], organometallic chemistry [14, 47], and other physical methods [48]. The organometallic chemical method can give a relatively high quantum yield with a very short lifetime of luminescence of Mn^{2+} ions.

In this research, the DMS quantum dots of CdS:Mn in polyvinyl alcohol (PVA) were synthesized by using a chemical method similar to that used for fabrication of undoped CdS by reacting a Na_2S with a mixture of Cd^{2+} and Mn^{2+} in aqueous solution. We also used two different methods to prepare DMS quantum dots.

The first method is as follows: reagents of 0.1 mM $CdCl_2$, 0.1 to 10 μ M of $MnCl_2$ and 0.01ml RSH (2-mercaptoethanol) were added into 10 ml of PVA saturated aqueous solution, while the solution was deoxygenated by N_2 gas and stirred by a magnetic stirrer. The prepared mixture was dried at 70℃ in a vacuum oven for several hours and then was casted on a glass plate. After that, it was dried further for 6 hours at the same temperature. Next, the glass plate was put in an aqueous solution of Na_2S and NaOH for 1 to 5 minutes. Then the plate was washed with distilled water and put in the vacuum oven to be dried again. Subsequently the PVA film of 10~80 μ m with CdS:Mn quantum dots was obtained. CdS quantum dot size can be controlled by altering the concentration of RSH or the reaction time with S^{2-}.

The second method is as follows: reagent solutions of 0.1 mM $CdCl_2$, 0.1 to 10 μ M of $MnCl_2$ and 0.005-0.05 ml RSH (2-mercaptoethanol) were added into 10 ml PVA saturated aqueous solution, while the solution was deoxygenated by N_2 gas and stirred by a magnetic stirrer. Next, the fresh Na_2S, NaOH aqueous solution was added to the mixture in the dark while the mixture being stirred by a magnetic stirrer, and stirred it for an hour. The resultant solution was dried in nitrogen atmosphere at 70℃ for more than 6 hours and then was cast onto a cover glass plate. The precursor film was dried further at 40 mmHg for one day.

CdSe:Mn and ZnSe:Mn quantum dots are fabricated similarly by the second method in this work, because the sodium selenide is much expensive than sodium sulfide, and is unstable in air.

2.2.3 Characterization of quantum dots

The size of quantum dots was determined by the small angle X-ray scattering (SAXS) measurement. The incident X-ray beam was elastically scattered by quantum dots and detected. The signal was analyzed using the Guinier's method. The scattered X-ray intensity is expressed as:

$$I(s) \propto \exp(-\frac{(2\pi s R_g)^2}{3}), \qquad s = \frac{2\sin(\theta)}{\lambda}, \tag{2.1}$$

where 2θ is the scattering angle, λ is the wavelength of X-ray, $R_g = \sqrt{\frac{3}{5}}R$, R is the average radius of quantum dots.

Reference

[1] Y. Kanemitsu, *Phys. Rep.* 263, 1-91 (1995), and the references there in.

[2] L. J. Geerligs, C. J. Harmans and L. P. Kouwenhoven (Eds.), The physics of few-electron nanostructures, *Physica* 189 B, No. 1 to 4 (1993).

[3] L. E. Brus, *J. Chem. Phys.* 80, 4403 (1984).

[4] R. Rossetti, R. Hull, J. M. Gibson, and L. E. Brus, *J. Chem. Phys.* 82, 552 (1985).

[5] A. P. Alivisatos, A. L. Harris, N. J. Levinos, M. L. Steigerwald and L. E. Brus, *J. Chem. Phys.* 89, 4001 (1988).

[6] C. B. Murray, D. J. Norris and M. G. Bawendi, *J. Am. Chem. Soc.* 115, 8706 (1993).

[7] D. J. Norris, A. Sacra, C. B. Murray and M. G. Bawendi, *Phys. Rev. Lett.* 72, 2612 (1994).

[8] M. G. Bawendi, W. L. Wilson, L. Rothberg, P. J. Carroll, T. M. Jedju, M. L. Steigerwald and L. E. Brus, *Phys. Rev. Lett.* 65, 1623 (1990).

[9] M. G. Bawendi, P. J. Carroll, W. L. Wilson, and L. E. Brus, *J. Chem. Phys.* 96, 946 (1992).

[10] C. B. Murray, M. Nirmal, D. J. Norris, and M. G. Bawendi, *Z. Phys.* D26, 231 (1993).

[11] Y. Wang, N. Herron, W. Mahler, and A. Suna, *J. Opt. Soc. Am.* B6, 808 (1989).

[12] Y. Wang, N. Herron, *J. Chem. Phys.* 95, 1119 (1991).

[13] K. Misawa, H. Yao, T. Hayashi, and T. Kobayashi, *Chem. Phys. Lett.* 183, 113 (1991).

[14] R. N. Bhargava, D. Gallagher, X. Hong and A. Nurmikko, *Phys. Rev. Lett.* 72, 416 (1994).

[15] U. Woggon, S. V. Bogdanov, O. Wind, K.-H. Schlaad, H. Pier, C. Klingshirn, P. Chatziagorastou and H. P. Fritz, *Phys. Rev.*. B48, 11979 (1993).

[16] J. Qi and Y. Masumoto, *Solid State Commun.* 99, 467 (1996).

[17] M. A. Hines and P. Guyot-Sionnest, *J. Phys. Chem.*. 100, 468 (1996).

[18] B. A. Korgel and H. G. Monbouquette, *J. Phys. Chem.*. 100, 346 (1996).

[19] Y. Wang and N. Herron, *J. Chem. Phys.* 92, 4988 (1988).

[20] K. Misawa, H. Yao, T. Hayashi, and T. Kobayashi, *J. Chem. Phys.* 94, 4131 (1991).

[21] J. E. Bowen Katari, V. L. Colvin, and A. P. Alivisatos, *J. Phys. Chem.* 98, 4109 (1994).

[22] O. I. Micic, J. R. Sprague, C. J. Curtis, K. M. Jones, J. L. Machol, A. J. Nozik, H. Giessen, B. Fluegel, G. Mohs and N. Peyghambarian, *J. Phys. Chem.* 99, 7754 (1995).

[23] A. A. Guzelian, J. E. B. Katari, A. V. Kadavanich, U. Banin, K. Hamad, E. Juban, A. P. Alivisatos, R. H. Wolters, C. C. Arnold and J. R. Heath, *J. Phys. Chem.* 100, 7212 (1996).

[24] A. A. Guzelian, U. Banin, A. V. Kadavanich, X, Peng, and A. P. Alivisatos, *Appl. Phys. Lett.* 69, 1432 (1996).

[25] A. Mews, A. V. Kadavanich, U. Banin, and A. P. Alivisatos, *Phys. Rev.* B 53, 13242 (1996).

[26] A. Mews, A. Eychmüller, M. Giersig, D. Schooss, and H. Weller, *J. Phys. Chem.*. 98, 934 (1994).

[27] L. Spahnel, M. Haase, H. Weller and A. Henglein, *J. Am. Chem. Soc.* 109, 5649 (1987).

[28] A. Eychmüller, A. Mews, and H. Weller, *Chem. Phys. Lett.* 208, 59 (1993).

[29] K. Sooklal, B. S. Cullum, S. M. Angel, and C. J. Murphy, *J. Phys. Chem.*. 100, 4551 (1996).

[30] J. Qi, T. Okuno and Y. Masumoto, *Proc. 2nd Asia Sym. Cond. Mat. Photophys.* 430 (Nara, 1996).

[31] I. Honma, T. Sano, and H. Komiyama, *J. Phys. Chem.* 97,6692 (1993).

[32] S. A. Blanton, A. Dehestani, P. C. Lin, P. Guyoy-Sionnest, *Chem. Phys. Lett.* 229, 317 (1994).

[33] S. A. Empedocles, D. J. Norris and M. G. Bawendi, *Phys. Rev. Lett.* 77, 3873 (1996).

[34] H. Yao and T. Hayashi, *Chem. Phys. Lett.* 197, 21 (1992).

[35] A. P. Alivisatos, T. D. Harris, P. J. Carroll, M. L. Steigerwald, and L. E.

Brus, J. *Chem. Phys.* 90, 3463 (1989).

[36] P. E. Lippens and M. Lannoo, *Phys. Rev.* B41, 6079 (1990).

[37] N. Herron, A. Suna and Y. Wang, *J. Chem. Soc. Daiton. Trans.* 15, 2329 (1992).

[38] A. I. Ekimov, Al. L. Efros and A. A. Onushenko, *Solid State Commun.* 56, 921 (1985).

[39] K. Kang, A. D. Kepner, Y. Z. Hu, S. W. Koch, N. Peyghambarian, C.-Y. Li, T. Takada, Y. Kao, and J. D. Mackenzie, *Appl. Phys. Lett.* 64, 1487 (1994).

[40] T. Takada, J. D. Mackenzie, M. Yamane, K. Kang, N. Peyghambarian, R. J. Reeves, E. T. Knobber, R. C. Powell, *J. Mater. Sci.* 31, 423 (1996).

[41] M. Nogami, Y. Zhu, Y. Tohyama, K. Nagasaka, T. Tokizaki, and A. Nakamura, *J. Am. Ceram. Soc.* 74, 238 (1991).

[42] F. Hatami, N. N. Ledentsov, M. Grundmann, J. Böhrer, F. Heinrichsdorff, M. Beer, D. Bimberg, S. S. Ruvimov, P. Werner, U. Gosele, J. Heydenreich, A. V. Ivanov, B. Ya. Meltser, P. S. Kop'ev and Zh. I. Alferov, *Appl. Phys. Lett.* 67, 656 (1995).

[43] P. M. Petroff anf S. P. Denbarrs, *Supperlattices and Microstructures* 15, 15 (1994).

[44] S. Takami, Y. Egashira, I. Honma and H. Komiya, *Appl. Phys. Lett.* 68, 1020 (1996).

[45] K. Yanata, and Y. Oka, *Supperlat. Microstr.* 15, 233-236 (1994).

[46] T. Miyasato and M. Tonouchi, Mater. Sci. Eng. B, *So. Sta. Mater. Adv. Technol.* B9, 195 (1991).

[47] R. J. Bandaranayake, M. Smith, J. Y. Lin, H. X. Jiang and C. M. Sorensen, *IEEE Trans. Mag.* 30, 4930 (1994).

[48] T. Yoshiue, H. Iwata, M. Kobayashi, Y. Kobayashi, S. Endo, *Proc. 2nd Asia Sym. Cond. Mat. Photophys.* 205 (Nara, 1996).

3 Persistent spectral hole burning in CdS quantum dots embedded in PVA

3.1 Introduction

Semiconductor quantum dots have received much attention during recent years as promising nonlinear media for optical processing, and as novel systems exhibiting quantum confinement of the elementary excitation of crystals [1-2]. When spectrally narrow light excites the materials having the inhomogeneously broadened absorption band, a spectral hole is formed at the position of the excitation photon energy in the absorption band. The hole burning spectroscopy is useful for investigating the electronic quantum states of quantum dots buried in the inhomogeneous broadening [3-9]. So far, it is believed that the inhomogeneous broadening comes from the size distribution and the spectral hole burning observed in semiconductor quantum dots is transient. Nevertheless, the persistent spectral hole burning (PSHB) phenomena have been widely observed in many kinds of semiconductor quantum dots, such as CuCl, CuBr and CdSe quantum dots embedded in glass and crystal matrixes recently [10-12]. This phenomenon shows that the semiconductor quantum dots may be the promising new materials for the frequency domain optical storage.

The PSHB phenomena of semiconductor quantum dots depend strongly on the environmental host as well as the guest, as generally known in PSHB phenomena of many guest-host systems [13]. We can guess the PSHB phenomena in the quantum dots embedded in the polymeric matrixes have another character. According to the reported

spectral hole burning phenomena of quantum dots embedded in polymeric matrixes [3-6], the observed spectral hole can be preserved for microsecond in the CdSe quantum dots embedded in polyvinyl butyral [5], or for subsecond in the CdS quantum dots embedded in the polymer [3]. This means that the phenomena are not transient [14] and that the persistent time depends on samples. However, the persistent time of microsecond or subsecond is very short, compared with the persistent time of several hours observed in quantum dots embedded in glass and crystals [10-12]. The question whether the hole burning phenomenon lasting for much longer time can be observed or not in semiconductor quantum dots embedded in the polymeric matrixes arises.

In this research, we have studied the PSHB of CdS quantum dots embedded in the polymeric matrix. Here, we report the sample-dependent spectral hole burning phenomena in CdS quantum dots. We have found that the persistent time of the hole burning depends on the composition ratio of Cd^{2+}/S^{2-} and discussed the possible mechanism of the PSHB phenomena.

3.2 Experiment

3.2.1 Sample

The samples, CdS quantum dots embedded in polyvinyl alcohol, are prepared by using two different methods, which have been described in Sec. 2.2. The sizes of quantum dots are evaluated using the small angle x-ray scattering measurement. The mean radii of CdS quantum dots are between 1.4 nm and 3.0 nm. Since the Bohr radius of exciton of

bulk CdS crystal is 3.0 nm, our samples belong to the strong confinement regime on the criteria given by Kayanuma [15].

3.2.2 Optical absorption measurements

The spectroscopic measurements were performed at room temperature and low temperatures, respectively. At room temperature, absorption spectra were measured with a Hitachi U-4000 spectrophotometer. At low temperatures, absorption spectra were measured using a setup shown in Fig. 3.1. A deuterium lamp or a halogen lamp was used as the light source. The samples were immersed in liquid nitrogen (77 K) or superfluid helium (2 K) in a dewer or put in a temperature variable cryostat with a temperature range of 12 — 300 K. The transmission light was dispersed by a 93 cm monochromator (SPEX 1702), and detected by an optical multichannel analyzer (OMA) or a cooled CCD system.

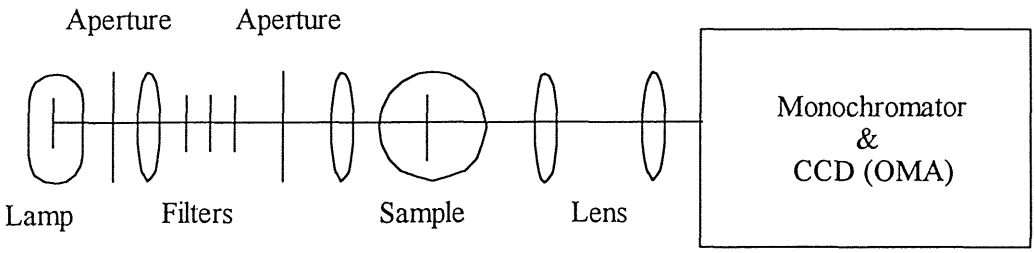

Fig. 3.1 Experimental setup for absorption spectral measurement at low temperature.

3.2.3 Photoluminescence measurements

The photoluminescence (PL) was measured using the setup shown in Fig. 3.2 at both room temperature and low temperatures. The excitation light source was the third harmonics of a Q-switched Nd^{3+}:YAG (yttrium aluminum garnet) laser pulse (5 ns) or the dye laser pulse pumped by it. The luminescence light was dispersed by a monochromator, and detected by a diode-array optical multichannel analyzer (OMA) or a cooled charge coupled device (CCD) system. The luminescence light was also detected by a photomultiplier, and averaged by a Boxcar integrator.

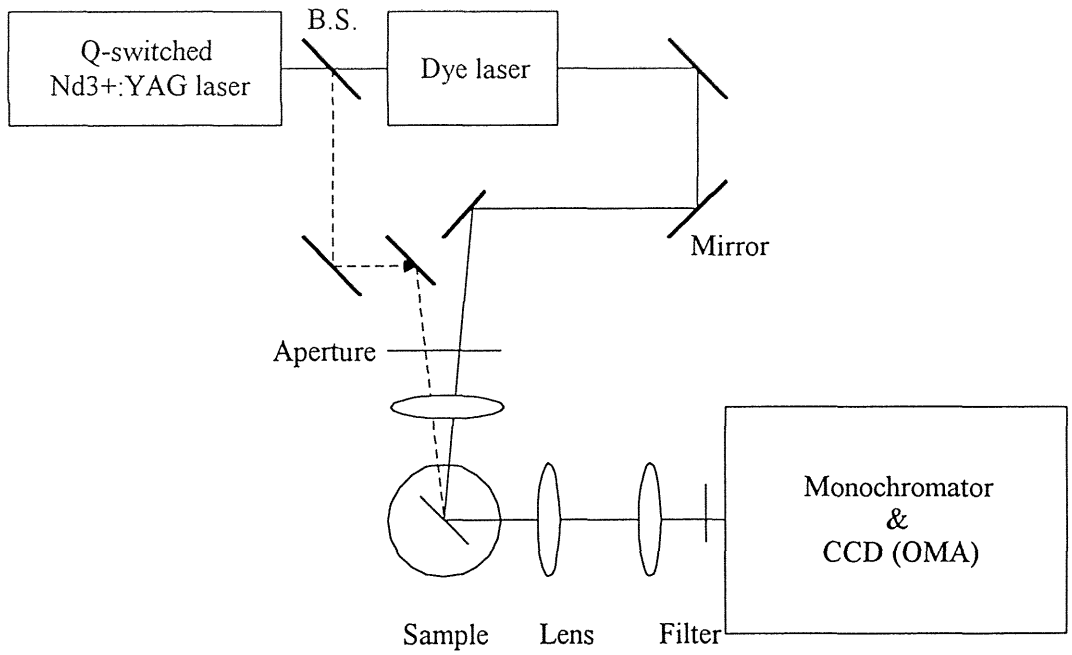

Fig. 3.2 Experimental setup for photoluminescence spectral measurements. Legend: B. S., beam splitter.

3.2.4 Nanosecond pump and probe measurements

The spectral hole burning measurements were done by using two kinds of setups according to the time regime of measurements. A narrow band dye laser pumped by the third harmonics of the output of a Q-switched Nd^{3+}:YAG laser was used to excite the sample selectively. The spectral line-width of the dye laser pulses was 0.003 nm and the pulse duration was about 5 ns. The first setup, shown in the Fig. 3.3, was used to measured the absorption change in the time regime shorter

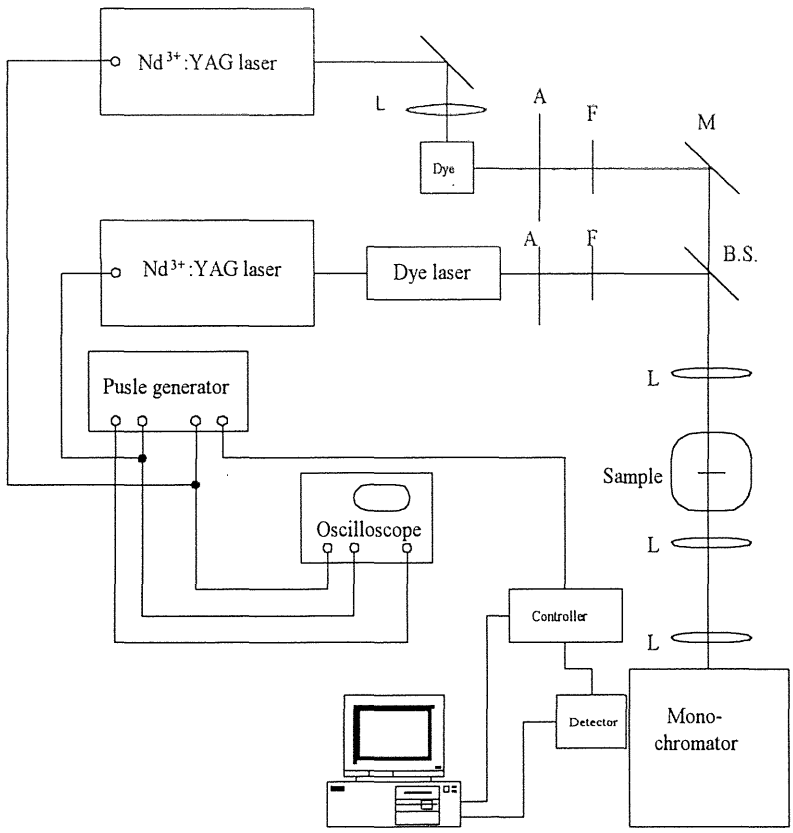

Fig. 3.3 Experimental setup for nanosecond pump-and-probe measurements. The time delay ranges from 0 to 0.1 s which is limited by the repetition rate of the dye laser. Legend: A, aperture; B.S., beam splitter; F, filter; L, lens and M, mirror.

than 0.1 s, the probe source was the amplified spontaneous emission light from the dye solution excited by the 5 ns laser pulse from another Q-switched Nd^{3+}:YAG laser. The time delay between two laser pulses of Nd^{3+}:YAG lasers was provided by a high-precision pulse generator (DG535, Stanford Res. Sys.). The delay time was set to range from zero to 0.1 s for the measurement of the spectral hole burning in this time regime. Another setup was used to measure the absorption change in the time regime longer than 1 min. The narrow band dye laser was used to excite the sample selectively and a halogen lamp was used as a probe source.

In the experiments, we first measured the absorbance $(\alpha d)_0$ of the sample without the pump laser beam, then measured the absorbance $(\alpha d)_{pump}$ at the arbitrary delay time after the pump, and got the differential absorption spectrum (DAS) of the sample. The absorption change can be expressed by the DAS, $-\Delta\alpha d = (\alpha d)_0 - (\alpha d)_{pump}$.

3.3 Results

The optical absorption and photoluminescence spectra are shown in Fig. 3.4. The absorption spectra are inhomogeneously broadened. The absorption thresholds show the blue shift due to the quantum size effect. The luminescence spectra obviously consist of two major components, and the luminescence peaks show a blue shift with the decrease of the quantum dot size. The shorter wavelength component is the recombination emission of excitons in the quantum dots, and the longer wavelength luminescence component is attributed to the radiative recombination of the localized carriers at the trap sites. The strong

longer wavelength luminescence suggests that there is a large relaxation rate to the trapped states for the excited electrons in the samples.

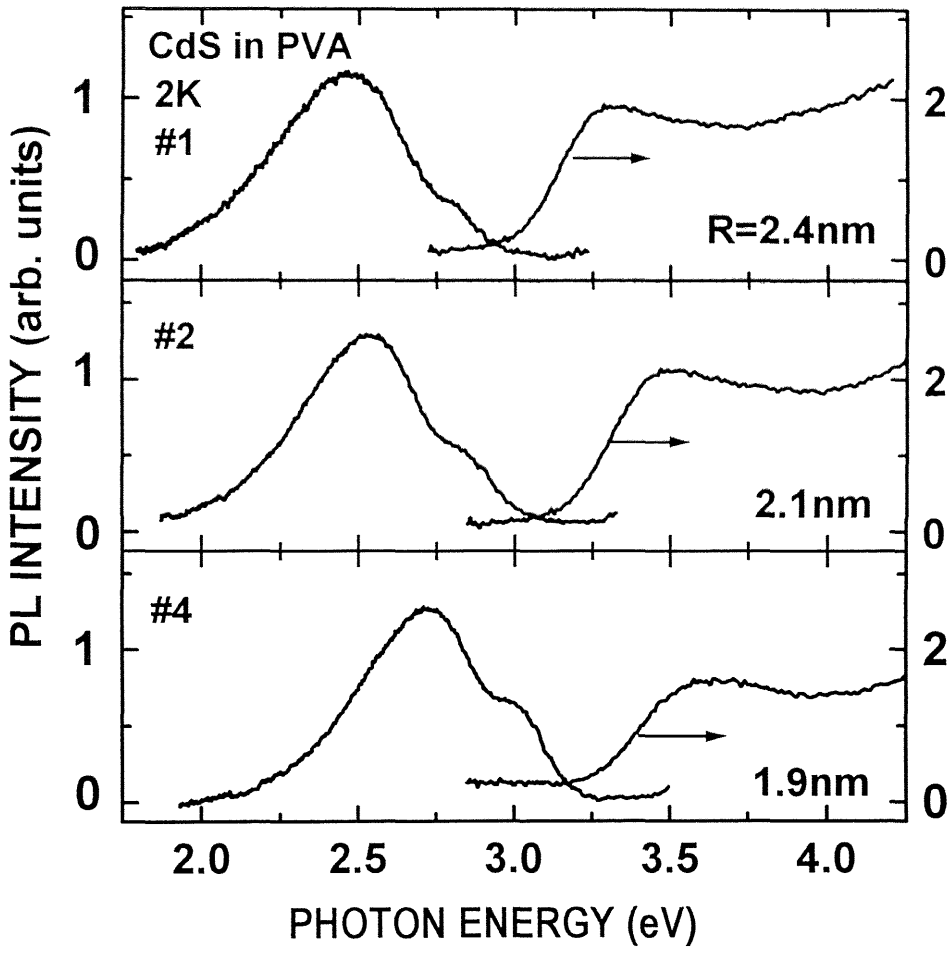

Fig. 3.4 Linear absorption spectra and photoluminescence spectra of 3 typical samples of CdS quantum dots embedded in PVA with the average radius of R=2.4, 2.1 and 1.9 nm, respectively, at 2 K.

The spectral hole burning we observed in the samples with rich S^{2-} ions has the shortest persistent time in all our samples. Figure 3.5 shows the spectral hole burning in the sample #1 at 14 K. We could not observe the burnt hole at the millisecond regime after the pump dye laser pulse hits the sample. However, in some samples containing nearly the same quantities of S^{2-} and Cd^{2+} ions, the spectral hole lasting for a very long time was observed, as shown in Fig. 3.6. The upper part of Fig. 3.6 shows the linear absorption spectra of the sample. The dashed line was the absorption spectrum of the virgin sample, while the solid one and the dotted one represent the absorption spectra measured at 0.2 μ s and 700 μ s after the laser the laser irradiation, respectively. The bleached dip shows a slight blue shift from the excitation energy. The full width at the half maximum (FWHM) of the hole is about 80 meV, which is nearly the same with that was observed in other CdS quantum dots [6,9]. The observed broad width of the hole is believed to come from the large electron-phonon coupling. The lower part shows the hole depth changes with the delay times. It shows that the spectral hole at 15 K can persist for as long as 100 ms after the laser irradiation. However, the hole structure disappears in the minute regime. The hole depth decays fast initially, and its decay becomes slower from 1 μ s after the excitation. This shows that there are the different decay processes at the different time stage.

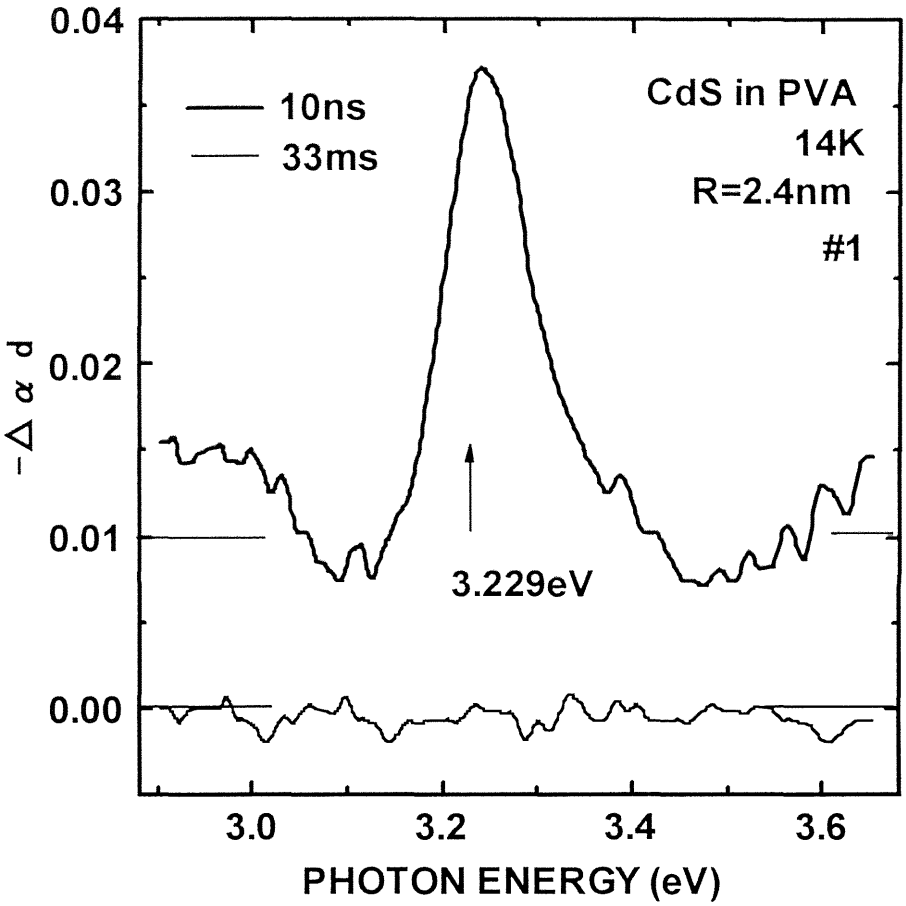

Fig. 3.5 Differential absorption spectra of the sample #1 at 14 K. The CdS quantum dots embedded in PVA were prepared by the first method described in the Sec.2.2. The pump laser photon energy is indicated by an upward arrow.

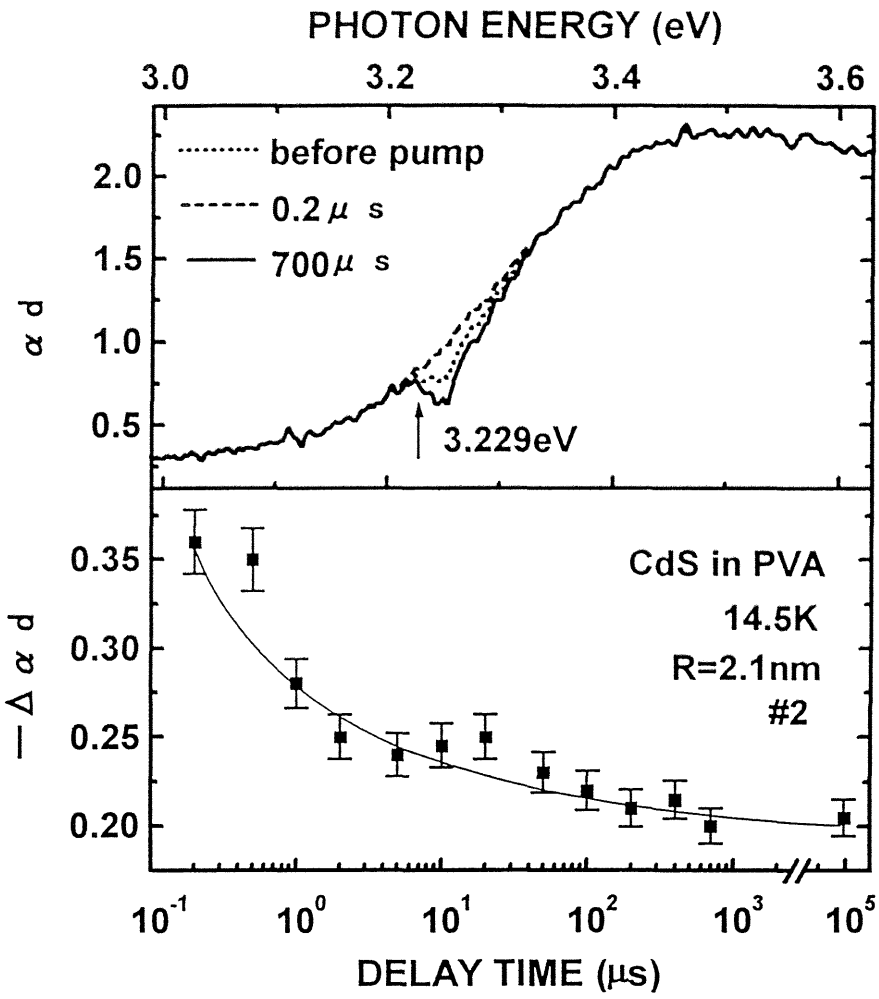

Fig. 3.6 Upper figure: Linear absorption spectra of the virgin sample and the laser-irradiated sample at different delay times after the pump at 15 K. Lower figure: the hole depth versus the delay times. The solid line is a guide to the eye. The excitation density and the laser repetition rate are 200 μ J/cm^2 and 10 Hz, respectively.

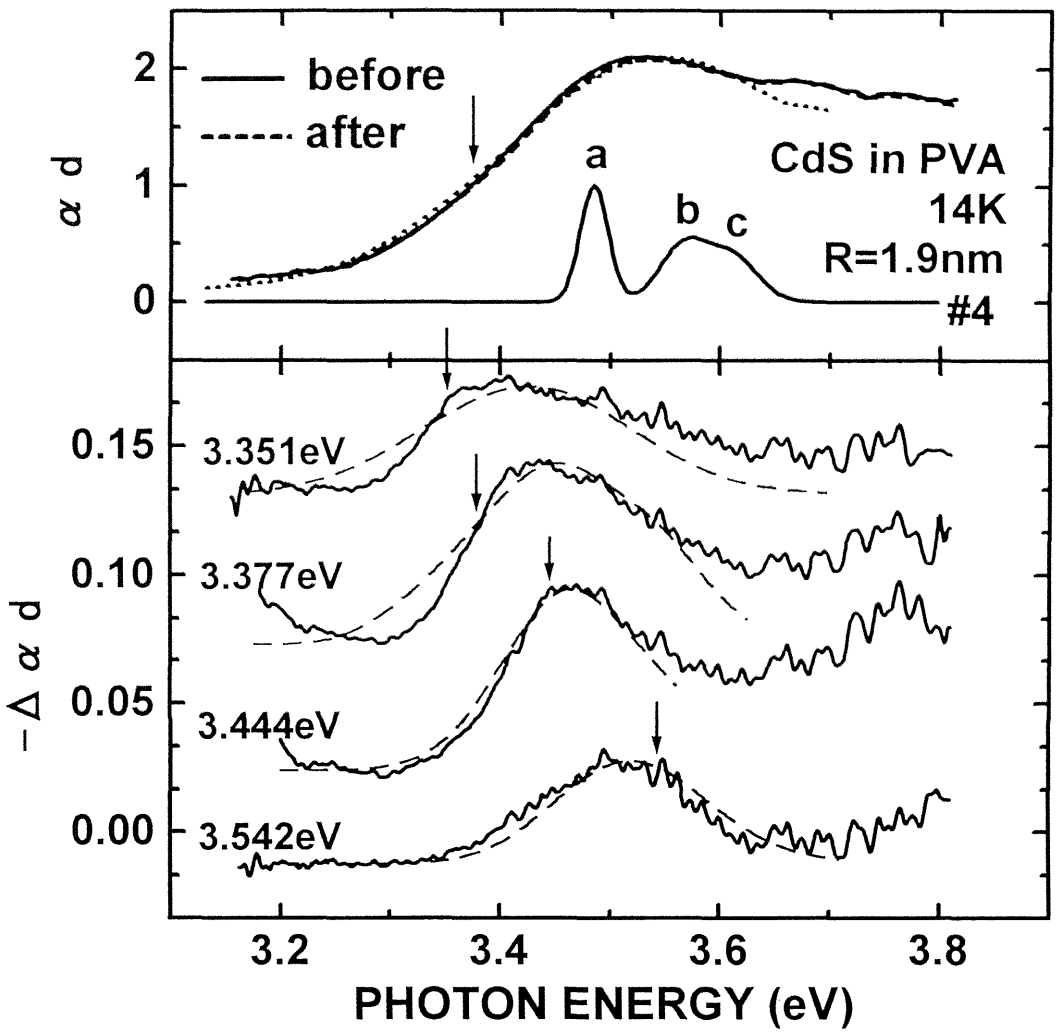

Fig. 3.7 Linear absorption spectra and differential absorption spectra of the sample #4, CdS quantum dots embedded in PVA prepared by the second method described in the text. Upper figure: the linear absorption spectrum of the virgin sample (solid line), the linear absorption of the laser-irradiated sample at 1 min after the laser excitation at 3.377 eV is stopped (dashed line), and the simulated result (dotted line). The excitation energy density and the number of shots are 500 μ J/cm^2 and 9000, respectively. Lower figure: the differential spectra (solid lines: experimental results; dashed lines: simulated results). The pump photon energies are shown by the downward arrows.

The persistent time of the spectral hole in CdS quantum dots embedded in polyvinyl alcohol matrix strongly depends on the sample. Figure 3.7 shows the persistent spectral hole burnt in the samples synthesized by the second preparation method that described in Sec. 2.2. The hole can be held for several hours. It also shows that the hole structure depends on the pumping photon energy. The bleached dip is not located at the excitation laser photon energy, but shows a slight red or blue shift depending on whether the laser photon energy is above or below the absorption shoulder, respectively. The PSHB of CdS quantum dots can be observed even at liquid nitrogen temperature. However, the bleaching hole structure is erasable when the temperature rises to 280 K. This observation is the longest persistent hole burning of the semiconductor quantum dots embedded in polymer matrix to our knowledge. According to the preparation method used here, there is a high probability of the free Cd^{2+} ions at the polymeric chains without S^{2-} ion counterparts. So it is considered that the PSHB observed in the samples is related to the excess Cd^{2+} ions of the samples. We also successfully observed PSHB lasting for more than 10 min in the samples with excess Cd^{2+} ions prepared by the first preparation method. Table 3.1 shows the persistent time of the burnt hole depending on the ratio of Cd^{2+}/ S^{2-} in the samples.

Table 3.1 CdS/PVA samples and the persistent time of their hole burning. Samples #1~#3 were prepared by the first method and the sample #4 was prepared by the second method. Persistent time means the time until the hole structure is held.

sample	radius (nm)	Cd^{2+}/S^{2-} ratio	HB persistent time
#1	2.4	0.947	$t < 33ms$
#2	2.1	1.000	$0.1s < t < 60s$
#3	2.1	1.103	$t > 10^2s$
#4	1.9	>1	$t > 10^3s$

3.4 Discussions

So far, we have successfully observed PSHB in CdS quantum dots with the persistent time of the burnt hole depending on the ratio of Cd^{2+}/S^{2-} in the samples. Here, we will discuss the mechanism of the observed PSHB phenomena.

Generally, if the preservation time of burnt spectral hole in a system longer than the excited lifetime of the sample, it can be considered as the PSHB. Basic requirements for the PSHB are as follows:

① The optical absorption of a guest embedded in a host must be broadened imhomogenously.

② There must exist more than one ground-state configurations of the total system consisting of a guest and a host.

③ The relaxation among the states must be slower than the decay of any excited state.

The microscopic mechanism leading to the PSHB phenomenon can be classified into two classes:

① Photochemical mechanism: Photochemical mechanism usually involves some internal changes in the guest itself, and the optical absorption from photochemical products can be observed in the linear absorption spectrum.

② Photophysical mechanism: Photophysical mechanism arises from the change in the surroundings of the guest.

The photophysical mechanism is observed in many systems of amorphous hosts. Figure 3.8 shows the schematic illustration of the photophysical PSHB mechanism based on the two-level-system model. The excited state, the initial ground state and the other ground states are represented by (E), (I) and (G), respectively. Site-selective excitation causes the transition from the initial ground state to the excited state and provides another ground-state configuration. The population at (G) is increased by the relaxation from (E). This causes the increase of the absorption at the both sides of spectral holes in the absorption spectrum. The relaxation time in the PSHB mechanism is mainly due to the relaxation from (G) to (I). The overall absorption area integrated over the inhomogeneously broadened spectrum should remain approximately constant, because the site-selective excitation redistributes the population among the ground states.

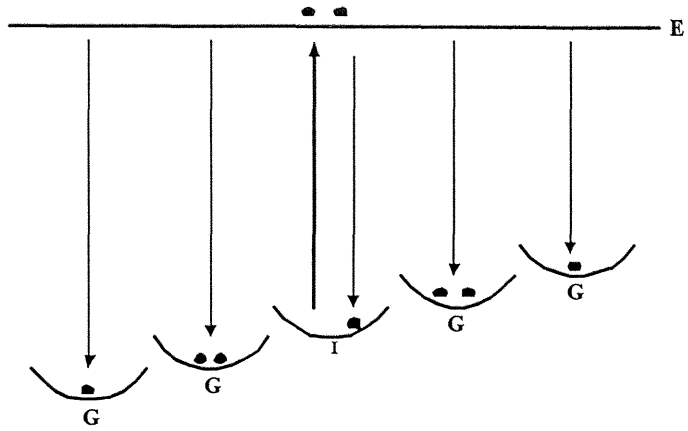

Fig. 3.8 The schematic illustration of the persistent spectral hole-burning phenomenon based on the photophysical mechanism. The excited state, the initial ground state and the other ground states are represented by (E), (I) and (G), respectively.

In the CdS quantum dots embedded in PVA, the observed HB persistent time depends on the ratio of Cd^{2+}/ S^{2-} in the samples. It is believed that the Cd^{2+} ions located around the CdS quantum dots or on the surface of the quantum dots can act as the electronic trap centers. According to the three-level-model [1], some excited electrons recombine fast with the valence hole. The other excited electrons can be captured by the trap centers through the tunnel process, and then relax to the ground state by radiative and nonradiative processes. If the all the excited electrons relax fast to the ground state, we can observe the transient HB only, not the PSHB. Similar to the PSHB in quantum dots embedded in the glasses and crystals [12], the possible mechanism may be as follows. When quantum dot is excited, an electron may escape from the quantum dot through the potential barrier in polymeric

host and is trapped at Cd^{2+} center in polymeric host. Photoionization of CdS quantum dots embedded in silicate glass has been clearly observed before [16]. Photoionized quantum dots and trapped electrons are stable enough to give PSHB at low temperature. There are many spatial arrangements for electrons and holes in both quantum dots and polymeric host. A variety of spatial arrangements induce an additional inhomogeneous broadening of the absorption spectra of CdS quantum dot. The presence of the inhomogeneous broadening coming from the carrier distribution configuration caused by the pumping light satisfies the requirement of the PSHB [13]. In Fig. 3.9, the schematic illustration of the proposed model is shown.

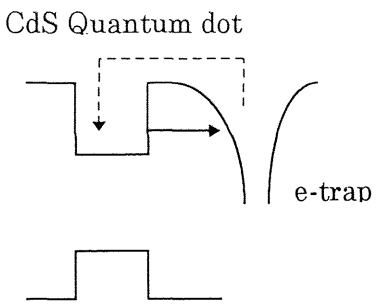

Fig. 3.9 Schematic model of the photo-ionization of CdS quantum dots embedded in PVA. Photogenerated electrons tunnel trough the barrier and are captured by traps (Cd^{2+}) in the host . The solid arrow and dashed arrow represent the electron tunneling process and hole-filling process induced by thermal annealing or light irradiation, respectively.

Since it is difficult to describe the PSHB starting from the quantum mechanics equation, instead of it, we give a semiclassical simulation of the phenomenon.

We simulated the experimental PSHB spectra following the procedure written in Ref. 17. The pump-induced bleached spectrum ($-\Delta\alpha d$) can be simulated by

$$-\Delta\alpha d(E) = C\int_0^\infty A(E-E_1)\{1-S(E_p-E_1)\}D(E_1-E_0)dE_1, \quad (3.1)$$

where E is the photon energy, $A(E-E_1)$ represents a dimensionless "single quantum dot" line shape function centered at E_1, $S(E_p\text{-}E_1)$ is a "saturation factor" which accounts for the decrease in absorption due to pump [17], $D(E_1\text{-}E_0)$ is a Gaussian inhomogeneous distribution centered at E_0 and C is an appropriate scaling factor. The saturation factor is given by

$$S(E_p-E_1) = \frac{1}{(1+I_R A(E_p-E_1))}, \quad (3.2)$$

where I_R is the ratio of pump light intensity to saturation intensity, and the inhomogeneous distribution function is normalized as,

$$\int_0^\infty D(E)dE = 1. \quad (3.3)$$

In the treatment of the single quantum dot absorption, we used the theoretically calculated results of Ref. 18, which considered the finite spin-orbit splitting effects on the optical properties of spherical quantum dots. The used single quantum dot line shape is shown in Fig. 3.7. The lowest three peaks labeled a-c correspond to the transitions between the electron state $1S_e$ and hole state $1SDD_{3/2}$, $2SDD_{3/2}$, and $3SDD_{3/2}$ respectively. Here, the integer numbers, in the hole states, are the principal quantum numbers, the first and the second capital letters indicate the types of the orbit state (S, P, D,...) which are mixed, the last capital letters correspond to the component related to the spin-orbit split-off states, and the subscript indices correspond to the value of total angular momentum. Two higher energy peaks separate from the lowest energy peak by 80 meV and 125 meV, according to the theoretical estimation of Ref. 18. First we use the convolution integral of the single quantum dot line shape function and the inhomogeneous distribution to

fit the linear absorption spectra. The fitting result is shown at the upper part of Fig. 3.7. The linewidths of peaks a-c are 30.4 meV, 50.2 meV and 55.5 meV, respectively; the relative oscillator strengths are 1, 0.77, 0.73, respectively. The width of inhomogeneous distribution is 300meV. Under the same condition, Eq. 3.1 was used to fit $-\Delta\alpha d$ spectra. The fitting results of $-\Delta\alpha d$ spectra are shown at the lower part of Fig. 3.7 by broad solid lines. The calculated differential absorption spectra agree with the experiments.

3.5 Conclusion

In summary, we have synthesized the CdS quantum dots embedded in polyvinyl alcohol polymer, and observed the persistent time of the hole burning depends on the molar ratio of Cd^{2+} / S^{2-} in the sample. In the samples with excess 10% Cd^{2+} ions, the observed hole structure lasted for several hours. In the sample whose Cd^{2+} / S^{2-} ratio is equal to or less than 1, the hole persistent time was less than 1 min. These observations suggest the following process as the PSHB mechanism. The excited electrons escape from the excited quantum dots and are trapped by the Cd^{2+} centers around the quantum dots in the polymer.

References

[1] L. E. Brus, *Appl. Phys.* A 53, 465 (1991).

[2] A. D. Yoffe, *Adv. Phys.* 42, 173 (1993).

[3] A. P. Alivisatos, A. L. Harris, N. J. Levinos, M. L. Steigerwald and L. E. Brus, *J. Chem. Phys.* 89, 4001 (1988).

[4] U. Woggon, S. Gaponenko, W. Langbein, A. Uhrig and C. Klingshirn, *Phys. Rev.* B 47, 3684 (1993).

[5] D. J. Norris, A. Sacra, C. B. Murray and M. G. Bawendi, *Phys. Rev. Lett.* 72, 2612 (1994).

[6] U. Woggon, S. V. Bogdanov, O. Wind, K.-H. Schlaad, H. Pier, C. Klingshirn, P. Chatziagorastou and H. P. Fritz, *Phys. Rev.* B 48, 11979 (1993).

[7] V. Esch, B. Fluegel, G. Khitrova, H. M. Gibbs, J. Xu, K. Kang, S. W. Koch, L. C. Liu and S. H. Risbud, *Phys. Rev.* B 42, 7450 (1990).

[8] E. F. Hilinski, P. A. Lucas and Y. Wang, *J. Chem. Phys.* 89, 3435 (1988).

[9] K. Kang, A. D. Kepner, Y. Z. Hu, S. W. Koch, N. Peyghambarian, C.-Y. Li, T. Takada, Y. Kao and J. D. Mackenzie, *Appl. Phys. Lett.* 64, 1487 (1994).

[10] Y. Masumoto, L. G. Zimin, K. Naoe, S. Okamoto, T. Arai, *Mater. Sci. Eng.* B 27, L5 (1994).

[11] K. Naoe, L. G. Zimin, Y. Masumoto, *Phys. Rev.* B 50, 18200 (1994).

[12] Y. Masumoto, S. Okamoto, T. Yamamoto, and T. Kawazoe, *Phys. stat. sol.* b 188, 209 (1995).

[13] W. E. Moerner (ed.), *Persistent Spectral Hole-Burning: Science and Applications* (Springer-Verlag, Berlin, Heidelberg, 1988).

[14] Classification as transient or persistent hole burning depends on whether the holding time of the hole is equal to or longer than the lifetime of the excited states; see Ref. [13].

[15] Y. Kayanuma, *Phys. Rev.* B 38, 9797 (1988).

[16] V. Ya. Grabovskis, Ya. Ya. Dzenis, A. I. Ekimov, I. A. Kudryavtsev, M. N. Tolstoi and U. T. Rogulis, *Soviet Phys.- Solid State* 31, 149 (1989).

[17] D. J. Norris and M. G. Bawendi, *J. Chem. Phys.* 103, 5260 (1995).

[18] T. Richard, P. Lefebvre, H. Mathieu and J. Allègre, *Phys. Rev.* B 53, 7287 (1996).

4 Photoluminescence of CdS:Mn quantum dots

4.1 Introduction

Diluted magnetic semiconductor (DMS) quantum dots belong to an attractive material system that combine both the semiconductor nanometer size confinement effect and magnetic finite size effects. Bhargava et al. recently reported the optical research on manganese-doped quantum dots of ZnS [1]. They found that the photoluminescence of Mn^{2+} ion in ZnS:Mn quantum dots has very high external quantum efficiency and its luminescence decays faster than that of Mn^{2+} in the bulk crystal by five orders of magnitude, suggesting that doped quantum dots are a new class of luminescent materials showing novel optical behaviors. Thus, it is expected that other DMS quantum dot systems may also have the similar optical properties. However, recent results on Mn^{2+} doped CdS quantum dots showed that the Mn^{2+} emission lifetime was not affected by quantum confinement, and it was similar to the Mn^{2+} emission lifetime in the bulk CdS host crystal [2]. This result is different from the Bhargava's observations. The reason of the so drastical difference in intrinsic properties of manganese is unimaginable, and is not known yet. Thus the luminescence properties of the DMS quantum dots need a further study. In this research, we have synthesized CdS:Mn quantum dots and investigated their optical properties. We focused on the behaviors of the Mn^{2+} luminescence. A high luminescence efficiency with a dramatically short lifetime (in the ns regime) was observed. Its excitation originates from the energy transfer from the host CdS quantum dots. We will give discussions on the possible mechanism on the Mn^{2+} luminescence.

4.2 Experiments

4.2.1 Sample

The DMS quantum dots in polyvinyl alcohol (PVA) were synthesized by using a chemical method by reacting a Na_2S with a mixture of Cd^{2+} and Mn^{2+} in aqueous solution. The details are described in the Sec. 2.2.

4.2.2 Photoluminescence measurements

The spectroscopic measurements were done at 2 K and room temperature. Absorption spectra were measured at the room temperature using a Hitachi U-4000 spectrophotometer, and at liquid nitrogen or liquid helium temperature using the setup shown in Fig. 3.1. The photoluminescence (PL) was measured using the setup shown in Fig. 3.2 at both room temperature and low temperatures. Photoluminescence excitation (PLE) measurements were performed by using two sets of 25 cm monochromators, an Ushio 500 W arc Xenon lamp as an excitation source and a photomultiplier tube for the detection of the PL. The experimental arrangement for PLE is shown in Fig. 4.1.

For quantum yield measurements, a rhodamine B dye solution of 10^{-6} M was used as a standard sample, its quantum yield is about 0.83 [3]. The quantum yield is calculated by:

$$\Phi_{pu} = \Phi_{ps}(K_s / K_u)(I_s / I_u)(n_u^2 / n_s^2)(A_u / A_s), \qquad (4.1)$$

where, Φ_p, K, I, A, n are the quantum yield, the absorbance at excitation wavelength, excitation intensity, luminescence intensity and the

refractive index, respectively; *u* and *s* represent the measured sample of the unknown quantum yield and the standard sample, respectively.

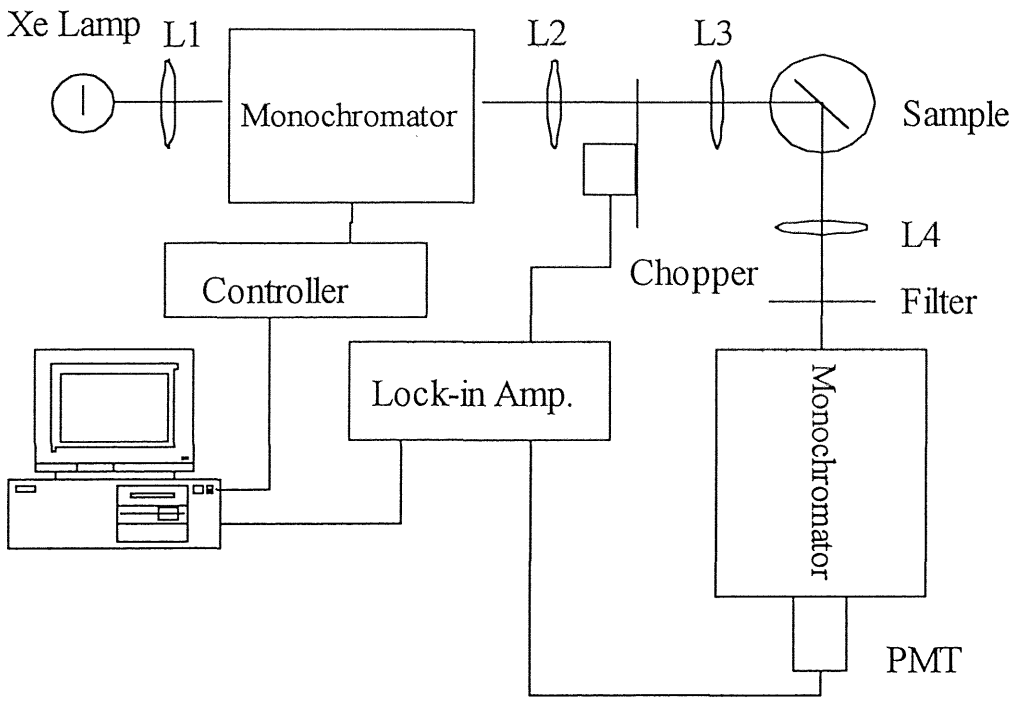

Fig. 4.1 Experimental setup for photoluminescence excitation spectroscopy.

4.2.3 Time resolved photoluminescence measurements

The PL decays were measured by a single photon counting method, using the 100 fs frequency-doubled pulses from a mode-locked Ti:sapphire laser as an excitation source. The pulse repetition was 250 kHz.

4.3 Results

4.3.1 Absorption and photoluminescence spectra

Figure 4.2 shows the optical absorption spectra and PL spectra of undoped and Mn^{2+} doped CdS quantum dots which are prepared in the same condition (i. e., the same quantities of reagents except the Mn

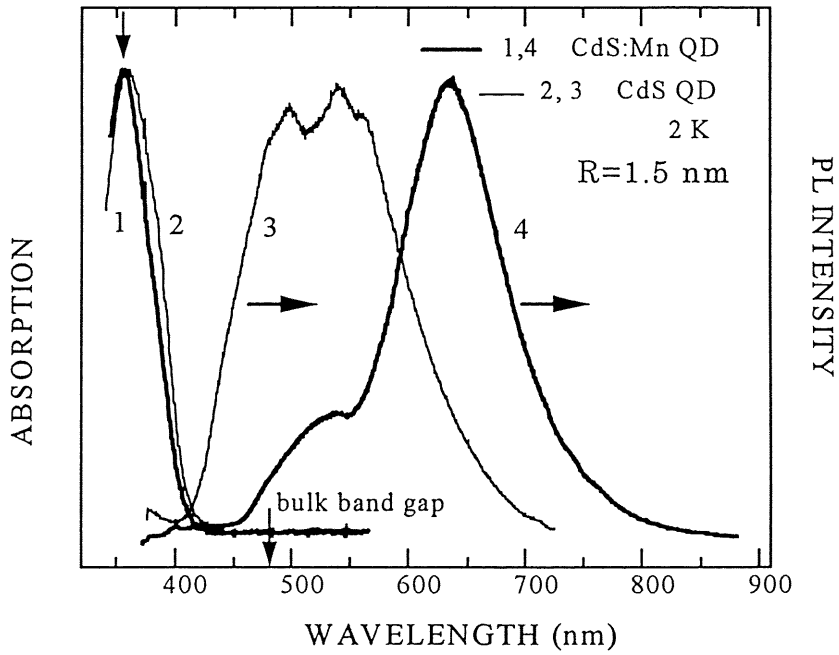

Fig. 4.2 Optical absorption spectra and PL spectra of undoped and Mn^{2+} doped CdS quantum dots at 2 K.

element, the same temperatures and the same sulphidation time as are used for the preparation of undoped CdS quantum dots). No obvious absorption components from d-d electron transitions of Mn^{2+} in CdS were observed in the absorption spectra. This is explained by considering that the concentration of Mn^{2+} ions is very low, and that only several Mn^{2+} ions are doped into a CdS quantum dot. In the bulk $Cd_{1-x}Mn_xS$ case, the absorption of Mn^{2+} ions is observed when x ~0.4 [4]. The observed absorption bands come from the transitions from the valence band to the conduction band in host CdS quantum dots. The blue shift of absorption peaks from the band gap of bulk CdS (E_g = 2.58 eV) is a direct evidence of the quantum confinement effect [5-6], which is the characteristic of quantum dots formed in the sample. Absorption spectra of Mn^{2+} doped and undoped CdS quantum dot samples are essentially similar to each other since the doping concentration is very low. Doping is effective only in altering the luminescence properties of the samples, but not the quantum dot size under the same synthesis conditions. A simple three-dimensional confinement model based on the effective mass approximation predicts the energy shift, ΔE, as [5-6]

$$\Delta E = \frac{\hbar^2 \pi^2}{2R^2}\left[\frac{1}{m_e^*}+\frac{1}{m_h^*}\right] - \frac{1.786e^2}{\varepsilon R} - 0.248E_{Ry}^* , \qquad (1)$$

where R is the quantum dot radius, m_e^*, m_h^* are the effective masses of electron and hole, respectively; ε is the dielectric constant, and E_{Ry}^* is the effective Rydberg energy, $e^4/2\varepsilon^2\hbar^2(1/m_e^*+1/m_h^*)$. Using m_e^*= 0.19 m_0, m_h^*= 0.8 m_0 and ε = 5.7 [6], we estimated the quantum dot size from the absorption data. For the sample with the absorption peak at 360 nm (3.444 eV or ΔE = 0.86 eV), the calculated value of R is 1.5 nm. It is a

little smaller than the value measured by means of the small angle X-ray scattering. The PL spectra of undoped CdS quantum dots show the green color emission bands from the trap centers on the surface of quantum dots with the peaks at 490, 540, and 570 nm. These peaks show a small shift with the size of quantum dots (i.e., absorption band edge), showing they come from the weakly localized trap states. However, the PL spectra of CdS:Mn quantum dots show a new orange emission components with a peak at 630 nm. This peak does not shift with the size of quantum dots, suggesting they come from deep localized centers. The emission is very strong and the greatest quantum yield is over 20% at room temperature. The strong luminescence is a unique character of our CdS:Mn quantum dots. We will discuss it at later part. This emission is attributed to Mn^{2+} ion $^4T_1 - ^6A_1$ transition in CdS host quantum dots, which is the result of s, p-d electron interactions between CdS host and Mn^{2+} impurity cations.

4.3.2 Excitation dependence of photoluminescence

Figure 4.3 shows PL spectra of undoped and Mn^{2+} doped CdS quantum dots under different excitation intensities at 2 K. The PL spectra of CdS quantum dots are broadened with the increase of excitation. On the other hand, the PL spectra of CdS:Mn quantum dots show the green trap PL component and orange Mn^{2+} PL component increasing with excitation by different rates (also see Fig.4.4). This fact again shows that orange and green luminescence components of CdS:Mn quantum dots come from the different luminescence centers.

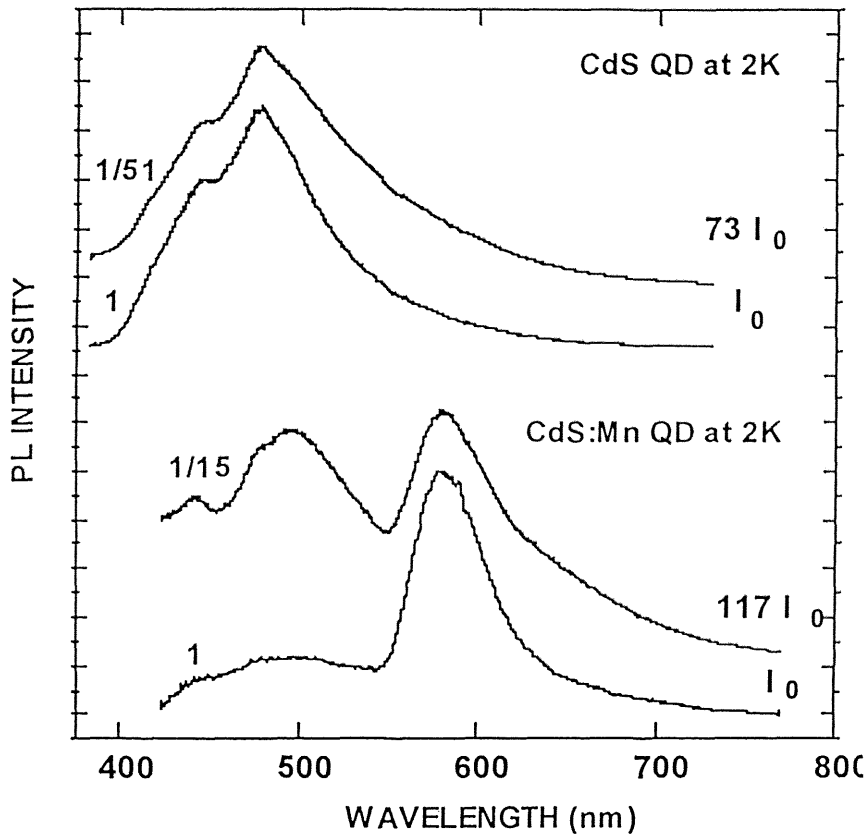

Fig. 4.3 PL spectra of undoped and Mn^{2+} doped CdS quantum dots under different excitation intensities at 2 K. Excitation laser wavelength is 384 nm.

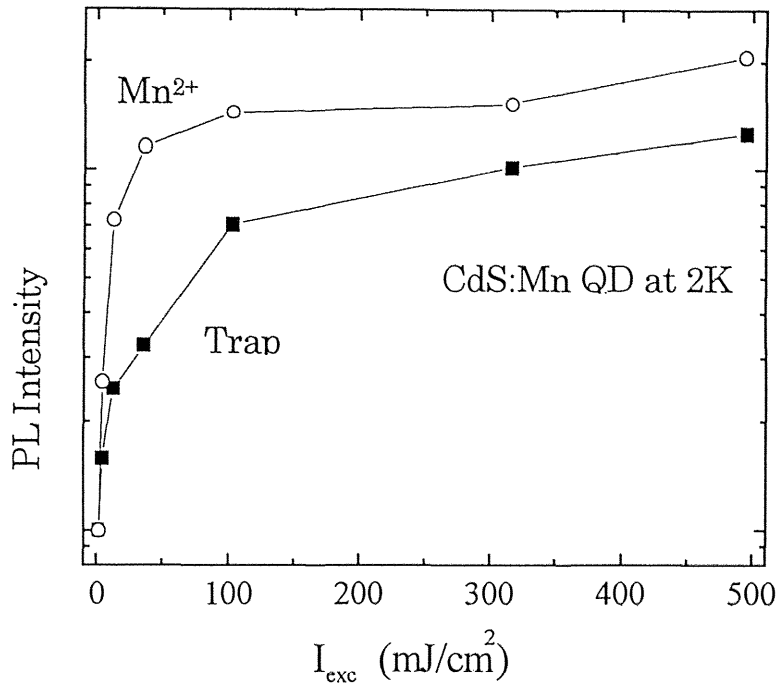

Fig. 4.4 The PL intensities (which are normalized to their values at the excitation of 1.5 mJ/cm^2) of Mn^{2+} ion and the trap site emission in CdS:Mn quantum dots versus excitation intensity. The excitation laser wavelength is 384 nm.

Figure 4.5 shows the PLE spectra probed at different luminescence wavelengths of undoped CdS quantum dots (upper part) and Mn^{2+} doped CdS quantum dots (lower part) at 2 K. The PLE spectra show that both the excitation bands of Mn^{2+} emission and the trap state emission originate from the band-to-band transition of host CdS quantum dots. Both the excitation spectra of the trap state emission and the Mn^{2+} emission are similar to the optical absorption spectra, and they are blue shifted obviously due to the quantum size effect compared with the bulk materials. No distinguished excitation spectrum feature coming from

Mn^{2+} 3d electron transition was observed at 510 nm ($^4T_1$), 486 nm ($^4T_2$) and 463 nm (^4E, $^4A_1$) (see Ref. [7]). However, when using the 514 nm, 488 nm lines of a cw Ar^+ laser to excite resonantly the Mn^{2+} in the quantum dots, the luminescence from Mn^{2+} can be observed, as shown in Fig. 4.6. These facts imply that the Mn^{2+} emission in CdS:Mn quantum dots are excited mainly through energy transfer from the band-to-band excited CdS quantum dots. It also means that the energy transfer to Mn^{2+} is more efficient than the Mn^{2+} direct excitation in CdS:Mn quantum dots.

The excitation energy transfer from CdS to Mn^{2+} can be also observed in bulk crystal materials. However, a larger spatial overlap of confined exciton wave-function with the localized d electron states of Mn^{2+} ions may occur in the quantum dots. The enhanced exchange interaction of s, p electrons with d electrons of Mn^{2+} in the quantum dots makes the energy transfer much faster than in the bulk state. In fact, we cannot observe the rise time of Mn^{2+} luminescence in our time-resolved measurement with the 50 ps time resolution.

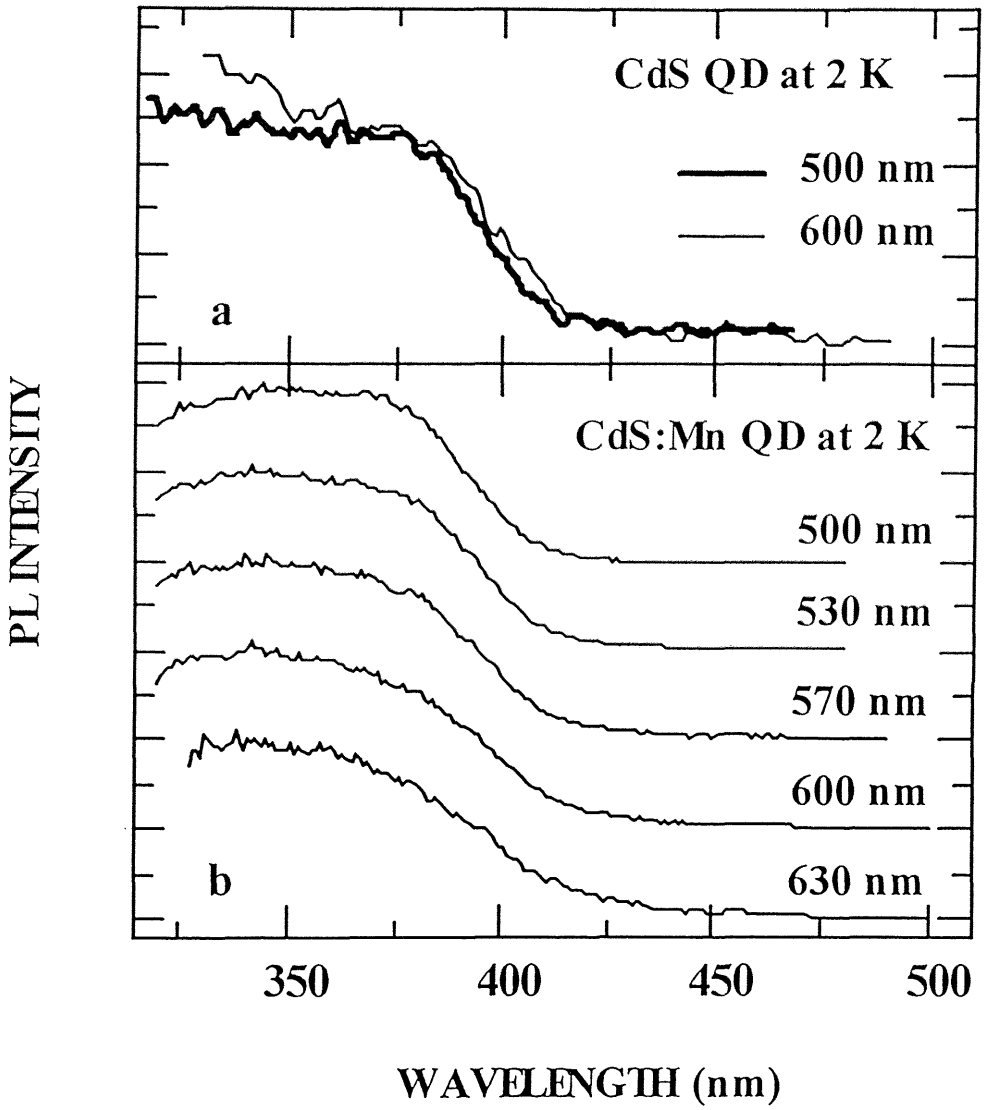

Fig. 4.5 Photoluminescence excitation spectra of (a) undoped and (b) Mn^{2+} doped CdS quantum dots at 2 K.

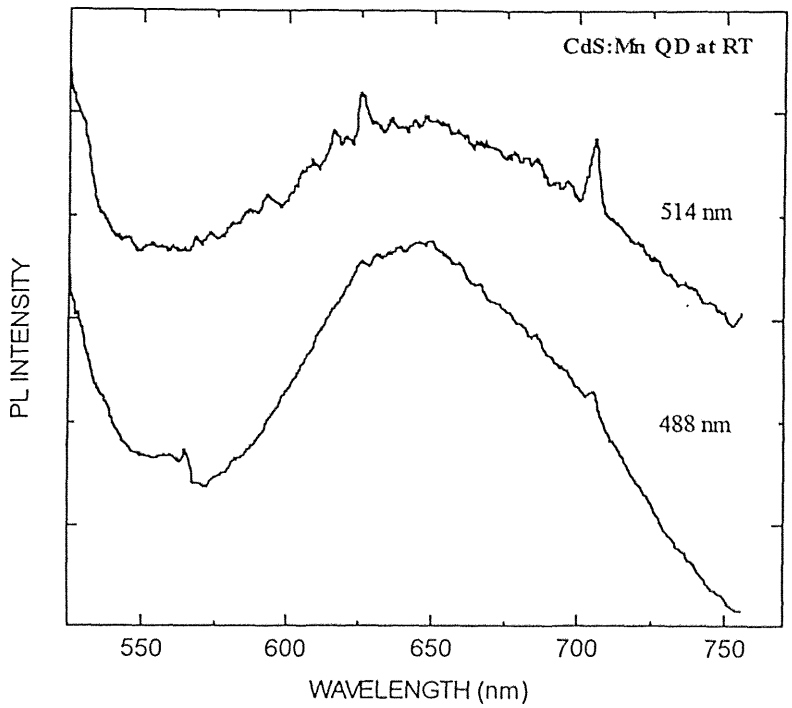

Fig. 4.6 PL spectra of Mn^{2+} doped CdS quantum dots resonantly excited by different wavelength line of an Ar^{+} laser at room temperature.

4.3.3 Luminescence decay

In this research, we have investigated the temporal decay properties of the Mn^{2+} luminescence. Figure 4.7 shows the measured luminescence decays of CdS:Mn quantum dots. Two-component exponential fit to the Mn^{2+} emission decay gave lifetime components on the order of ns. The 620 nm luminescence has 5.0 ns and 46 ns components of the emission lifetime. The PL decay of Mn^{2+} cannot be fit by a single exponential function. This implies the PL relaxation process of Mn^{2+} d electrons is

complex. However, It should be noted that this luminescence decays much faster than the corresponding one of millisecond order of lifetime in the bulk [2,8]. This observation is similar to the observation on the Mn^{2+} PL decay in ZnS:Mn quantum dots [1], in ZnTe/MnTe quantum wells [9], and Cu^{2+} PL decay in ZnS:Cu quantum dots [10], where the PL lifetimes of doped impurities in the nanostructures are shorter than the corresponding ones in the bulk structures. However, it is different from the observation on CdS:Mn quantum dots in glass [2], which shows the Mn^{2+} emission lifetime is not affected by the quantum confinement, and is nearly the same as the PL lifetime of millisecond order in the bulk CdS:Mn.

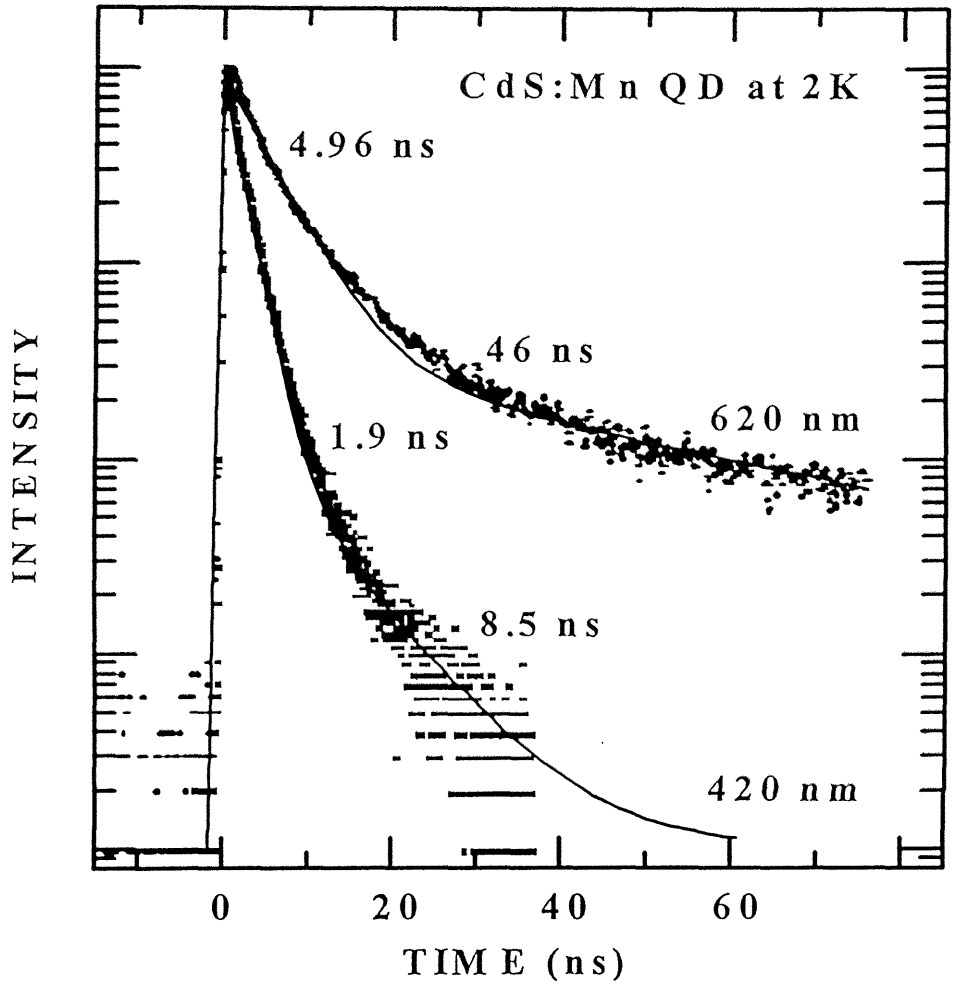

Fig. 4.7 The photoluminescence decay of Mn^{2+} doped CdS quantum dots at 2 K. The dots show the experimental results, and the solid lines show the results obtained by two-component exponential fitting.

4.4 Discussions

In the previous parts, we have shown that CdS:Mn quantum dots were successfully synthesized by the aqueous chemical method. The absorption spectra of CdS:Mn quantum dots show the blue shifts due to the quantum confinement effect. However, no absorption band of Mn^{2+} cations was observed because the low Mn^{2+} doping concentrations. The strong Mn^{2+} emission band associated with the 3d electron $^4T_1 - {}^6A_1$ transition was observed, and its lifetime is in the ns regime. The high quantum yield and short lifetime are two most remarkable characters of the Mn^{2+} emission in our CdS:Mn quantum dot sample. PLE observations show Mn^{2+} emission is excited through the energy transfer from the host CdS quantum dots to the internal Mn^{2+} levels. In the following parts, we discuss the possible mechanism of the observed Mn^{2+} emission in CdS:Mn quantum dots.

4.4.1 Mn^{2+} emission efficiency

As shown in Fig. 4.8 (b), the possible physical processes happened in the photo-excited CdS:Mn quantum dots are:

$$S_0 + h\nu \longrightarrow S_1, \qquad \text{absorption} \qquad (4.2)$$

$$S_1 \xrightarrow{k_{R0}} S_0 + h\nu_1, \qquad \text{exciton emission} \qquad (4.3)$$

$$S_1 \xrightarrow{k_{T1}} T^*, \qquad \text{carrier trapping} \qquad (4.4)$$

$$S_1 \xrightarrow{k_{T2}} Mn^*, \qquad \text{energy transfer to } Mn^{2+} \qquad (4.5)$$

$$S_1 \xrightarrow{k_{nr1}} S_o + h\omega, \qquad \text{nonradiative relaxation of } S_1 \qquad (4.6)$$

$$T^* \xrightarrow{k_R} S_0 + h\nu_2, \qquad \text{trap state emission} \qquad (4.7)$$

$$T^* \xrightarrow{k_{nr2}} S_0 + h\omega, \qquad \text{nonradiative relaxation of T}^* \qquad (4.8)$$

$$Mn^* \xrightarrow{k_r} Mn + h\nu_3, \qquad \text{Mn}^{2+} \text{ emission} \qquad (4.9)$$

$$Mn^* \xrightarrow{k_{nr3}} Mn + h\omega, \qquad \text{nonradiative relaxation of Mn}^{2+} \qquad (4.10)$$

The quantum yield is defined as the ratio of the emission photon number to the absorbed photon number. For Mn^{2+} emission in CdS:Mn quantum dots, the quantum yield of Mn^{2+} emission can be expressed as

$$\Phi_{Mn} = \frac{k_r}{k_r + k_{nr3}} \cdot \frac{k_{T2}}{k_{R0} + k_{nr1} + k_{T1} + k_{T2}}, \qquad (4.11)$$

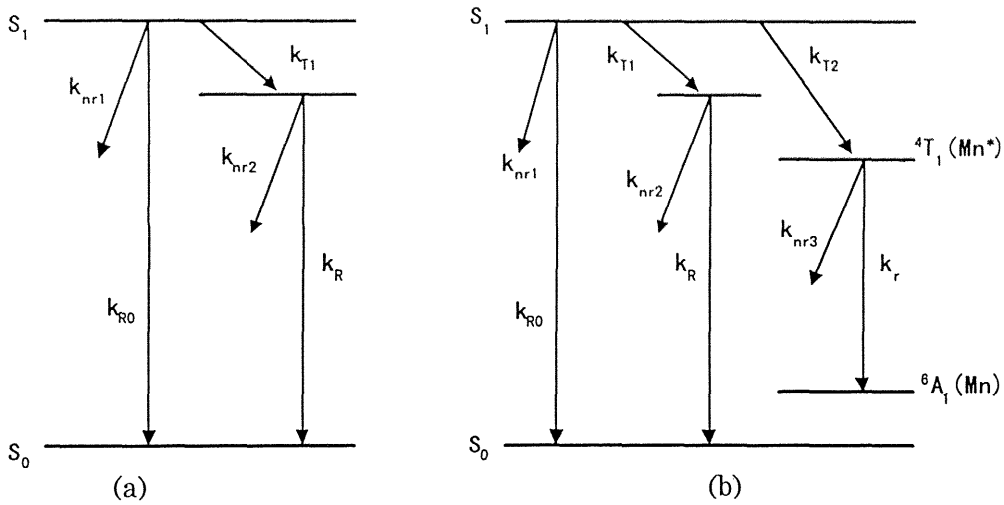

Fig.4.8 Schematic energy level diagrams for (a) undoped and (b) Mn^{2+} doped CdS quantum dots. The solid and dashed arrows indicate the radiative and nonradiative transitions, respectively.

where k_r, k_R and k_{R0} are the radiative recombination rates of Mn^{2+} ion, trapped carrier and exciton, respectively; k_{nr} is the nonradiative recombination rate. From the Eq. (4.11), we can see there are several ways to increase the Φ_{Mn}, i. e., the increase of k_r (shortening of the lifetime τ_r), k_{T2} (energy transfer rate from CdS to Mn^{2+}) and the decrease

of k_{nr1}.

We believe that the high quantum yield of Mn^{2+} emission canbe explained by these three reasons.

The first reason is the increase of k_r (shortening of the lifetime τ_r) of Mn^{2+} emission. This is true since we have experimentally observed the remarkably short lifetime of Mn^{2+} emission in CdS:Mn quantum dots compared to the corresponding one in the bulk CdS:Mn crystal.

The second reason is the increase of the energy transfer rate from CdS to Mn^{2+} , which will be discussed in 4.4.3.

The third reason is the decrease of k_{nr} caused by the surface passivation.

In the samples we used, the whole amount of Mn element in the reagent cannot be doped into CdS quantum dots. It is believed that the Mn cations can exist in the PVA matrix, on the surface of quantum dots or inside the quantum dots. Mn^{2+} cations inside the quantum dots substitute the Cd^{2+} cation site, and receive the excitation energy of CdS. The Mn^{2+} cations located on the surface of quantum dots and in the polymer matrix are believed to be existing in the form of MnS and $Mn(OH)_2$. As the results, the surfaces of CdS:Mn quantum dots are passivated by MnS, $Mn(OH)_2$, $Cd(OH)_2$, and PVA, then the energy transfer to nonradiative surface defects (e.g., the Cd^{2+} , S^{2-} vacancies) is weakened, i.e., the k_{nr} is decreased. So the surface passivation effect is another reason to cause the high radiative efficiency of CdS:Mn

quantum dots. Since MnS band gap equals to 3.75±0.1 eV [7], which is much larger than the band gap of bulk CdS of 2.58 eV, or the absorption edge of CdS:Mn quantum dots of 3.444 eV, no luminescence from MnS on quantum dot surface or in the PVA matrix can be observed for our experimental excitation energy less than 3.492 eV. $Mn(OH)_2$, $Cd(OH)_2$, and PVA also passivate the surface and cause the decrease of k_{nr} in the same way. The passivation of the quantum dot surface is a very effective way to increase the emission efficiency of the quantum dots. For example, the wide band ZnS-capped CdSe quantum dot exhibits strong band edge luminescence with a 50% quantum yield at room temperature [11]. It is the highest emission quantum yield of quantum dots so far reported at room temperature. Using this kind of sample, the single quantum dot luminescence spectra have been studied recently [12-13].

Therefore, we can conclude that the surface effects are very important to the luminescence properties of many kinds of quantum dots as well as the Mn^{2+} doped quantum dots.

The existence of a large number of surface defects maybe the most important reason why some authors observed the weak Mn^{2+} luminescence [14-15]. Another reason may be the concentration effects. The Mn^{2+} luminescence intensity increased with the increase of the concentration of Mn^{2+} cations, but the intensity was decreased by concentration quenching effect when Mn^{2+} concentration is above 0.12 at. wt %[16].

The problem how the Mn^{2+} luminescence influenced by the Mn^{2+} cation locations was also studied by other authors. Sooklal et al. have

found that neither the luminescence from the surface trap states nor from the Mn^{2+} ions can be observed, when the ZnS quantum dot was capped with Mn^{2+} ions [17]. However, when the Mn^{2+} ions are doped into the quantum dot, the luminescence from the $^4T_1 - ^6A_1$ transition of Mn^{2+} ions can be observed. Soo et al. also studied the local structure around Mn^{2+} luminescence centers in ZnS by X-ray absorption fine structure measurements. They found that the Mn^{2+} ions substitute the Zn^{2+} site in the host ZnS and that the substitution induces size dependent local structural changes [18]. Taking account of these studies and the fact that MnS and $Mn(OH)_2$ cannot be excited in our case, we believe that the observed Mn^{2+} emission in our CdS:Mn quantum dot samples comes from the Mn^{2+} ions inside CdS quantum dots (Fig.4.8).

4.4.2 Mn^{2+} emission lifetime

The short lifetime is another remarkable character of the Mn^{2+} emission in our CdS:Mn quantum dot sample. We will discuss it in this part.

In the bulk $A^{II}_{1-x}Mn_xB^{VI}$ DMS materials, Mn^{2+} cation replaced the A^{2+} cation site. The characteristic Mn^{2+} luminescence comes from the Mn^{2+} $3d^5$ electron $^4T_1 \rightarrow ^6A_1$ transition. This is a spin forbidden transition in the free-ion states, but in crystals the forbiddenness is partially broken owing to crystal field perturbation, phonon coupling and also to spin-orbit interaction. Its oscillator strength is about 10^{-5} or smaller than it. Typical lifetime is in the millisecond order.

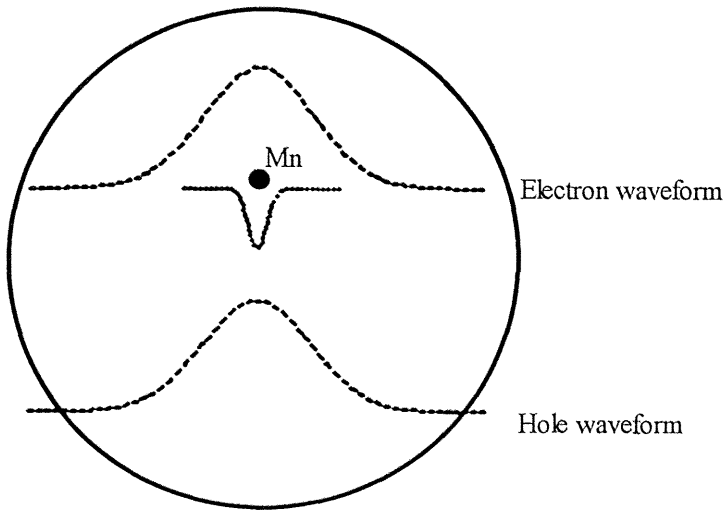

Fig. 4.9 A model depicting the overlap of electron-hole wave-function with a localized impurity potential in a quantum dot.

The fast transition rate (or short lifetime) of the Mn^{2+} $^4T_1 \rightarrow {}^6A_1$ transition in CdS:Mn quantum dots, can be explained, if the parity selection rule ($\Delta S = 0$) is broken in the quantum dots because of a large spatial overlapping of exciton wave-function with the Mn^{2+} 3d electron wave-function (Fig 4.9). The strong sp-d mixing in the quantum dots results in the fast decay time of Mn^{2+} ions.

This is the reason why Mn^{2+} $^4T_1 \rightarrow {}^6A_1$ transition lifetime is greatly shortened in CdS:Mn quantum dots. This reasoning can also be applied to explain the similar observations in other systems, e.g., the Mn^{2+} $^4T_1 \rightarrow {}^6A_1$ transition lifetime (ns) in the ZnS:Mn quantum dots [1], the Cu^{2+} transition lifetime (ns) in the ZnS:Cu quantum dots [10], and the Mn^{2+} $^4T_1 \rightarrow {}^6A_1$ transition lifetime (μs) in the ZnTe/MnTe quantum well [9].

4.4.3 Energy transfer mechanism

Here, we discuss the mechanism of the energy transfer from CdS to Mn^{2+} in CdS:Mn quantum dots. First of all, the resonant energy transfer condition is satisfied by the overlap between the emission band of CdS quantum dots and the absorption band of Mn^{2+}. Next, we see the several resonant energy transfer models proposed by Dexter [19] and Förster [20] can be applied to the energy transfer to Mn^{+2} in the quantum dots.

① Excited charge transfer: Mn^{+2} has a half-filled $3d^5$ structure. All five 3d electron spins are parallel to each other in the 3d orbit and form a stable structure. Mn^{+2} is electrically neutral in $A^{II}_{1-x}Mn_xB^{VI}$ structures, i.e., it constitutes neither an accepting nor a donating center. The energy transfer cannot work through the electron transfer between a CdS donor and a Mn^{+2} ion acceptor. Therefore, the electron transfer mechanism is excluded.

② Electric multipole interaction: The energy transfer through electric multipoles interaction may be a way of energy transfer from CdS to Mn^{2+} in CdS:Mn quantum dots, i.e., the exciton dipole interacts with dipole of Mn^{2+}, and passes its excited energy to the later. The probability of energy transfer between a pair of a donor and an acceptor through the dipole-dipole interaction is expressed as [19]:

$$P_{DA}(dd) = \frac{3c^4\hbar^4}{4\pi n^4 L^6} \cdot \frac{\sigma_A}{\tau_A} \int \frac{f_D(E)F_A(E)}{E^4} dE, \qquad (4.12)$$

where, n, σ and τ are the refractive index, absorption cross section and the radiative lifetime, respectively; $f(E)$ and $F(E)$ are

the emission spectral shape of a donor and the absorption spectral shape of an acceptor, respectively; L is the distance between a donor and an acceptor. Similarly, the probability of energy transfer between a pair of donor and acceptor through the dipole-quadrupole interaction is expressed as:

$$P_{DA}(dq) = \frac{135\pi\alpha c^8\hbar^9}{4n^6\tau_D\tau_A L^8}\int\frac{f_D(E)F_A(E)}{E^8}dE,$$

$$(\alpha = 1.266). \qquad (4.13)$$

The dipole-quadrupole and quadrupole-quadrupole interaction are much weaker than the dipole-dipole interaction when the donor and the acceptor are distant from each other. Since the dipole transition in the acceptor (Mn^{2+}) is partially forbidden in bulk, the dipole-dipole energy transfer may be very weak in bulk. Moreover, the dipole-quadrupole and quadrupole-quadrupole interaction (the energy transfer probabilities of these processes have the dependencies of L^{-8} and L^{-10}) also do not play as the key roles in the bulk crystal, since Mn^{2+} ions and the excitons are randomly dispersed in the crystal, the average distance between exciton and Mn^{2+} may be very long.

The situation is changed in the quantum dots. Firstly, the transition between the Mn^{2+} internal energy levels is allowed, i.e., the dipole-dipole interaction may be an active process. Secondly, all the excited exciton dipole, quadrupole of exciton, and dipole or quadrupole of Mn^{2+} cations are confined in the same quantum dot. The multipole interaction in CdS:Mn quantum dots may be enhanced compared to that of the bulk crystal. Therefore, the multipole interaction may be one reason causing the energy

transfer from CdS to Mn^{2+} in CdS:Mn quantum dots.

③ Exchange interaction: When the energy donor is adjacent to the acceptor spatially, its wave-function (electron cloud) is overlapping with that of the acceptor (see Fig. 4.10). It is possible to transfer energy through the quantum exchange interaction. If the overlapping of wave-functions is expressed by $K\exp(-\frac{L}{R})$, the energy transfer probability can be expressed as [19],

$$P_{DA}(ex) = K^2(\frac{2\pi}{\hbar})\exp(-\frac{2L}{R})\int f_D(E)F_A(E)dE, \qquad (4.14)$$

where, R is effective Bohr radius (i.e., the average effective Bohr radius between the donor excited state and the acceptor ground state), $K=3$ is a dimensional factor. Since there is not a term of absorption cross section in Eq. (4.14), the exchange interaction can cause the energy transfer from the donor to the acceptor when they are spatially adjacent to each other, even if the light absorption by the acceptor is forbidden. For this reason, the exchange interaction process may be the key process of the energy transfer from CdS to Mn^{2+} in the bulk crystal. In a quantum dot of the strong confinement condition, all the exciton wave-functions are confined in the quantum dot, the overlapping of the wave-functions between the s, p electronic states of exciton and d states of Mn^{2+} is increased. As a result, the transfer rate was enhanced in the quantum dots.

Therefore, we believe that the electric multipole interaction and exchange interaction mechanisms transfer the excited energy of CdS to Mn^{2+} in CdS:Mn quantum dots. This is different from the bulk case, where only the exchange interaction mechanism works. Both the electric multipole interaction and exchange interaction are enhanced

due to the quantum confinement. These interaction mechanisms result in a large energy transfer rate, a fast rise time of Mn^{2+} (see Fig. 4.7) and a high quantum yield of Mn^{2+} emission.

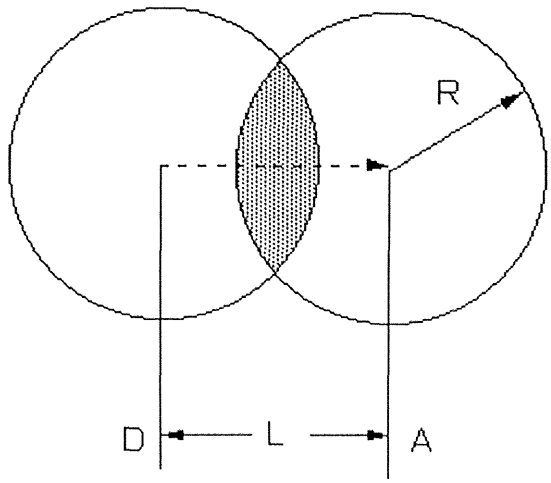

Fig. 4.10 A model depicting the resonant energy transfer through the exchange interaction. The shadow part shows the overlapping of electron clouds of a donor and an acceptor.

4.4.4 PSHB in CdS:Mn quantum dots

The PSHB in CdS:Mn quantum dot samples has been measured, too. A typical result is shown in the Fig. 4.11. The spectral hole burning can be observed at 1 min after the laser irradiation. Similarly to the PSHB in CdS quantum dots (see Sec. 3), the PSHB in CdS:Mn quantum dots can also be explained by the photoionization of quantum dots, i.e., a part of the excited carriers are trapped in the surrounding matrix. However,

experimentally, it needs much more laser fluence to generate a spectral hole in CdS:Mn quantum dots than that needed for generating a same depth hole in CdS quantum dots. This is understood as follows.

Due to the existence of a strong energy transfer path to the Mn^{2+} ions, the number of the carriers being trapped by the trap sites in the surrounding matrix is decreased in the photoexcited CdS:Mn quantum dots compared to that of CdS quantum dots. Moreover, since a Mn^{2+} ion has a very short lifetime, it cannot contribute to the PSHB. Thus, it is difficult to generate the persistent spectral hole in CdS:Mn quantum dots than in CdS quantum dots.

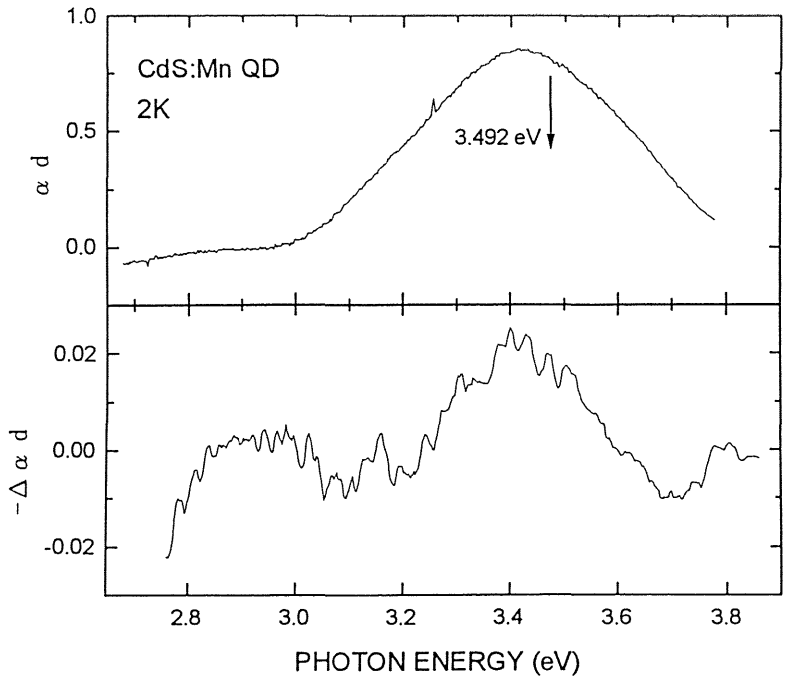

Fig. 4.11 Upper figure: the linear absorption spectrum of the virgin sample. Lower figure: the differential absorption spectrum at 1 min after the laser irradiation is stopped. The pump laser photon energy is indicated by a downward arrow. The excitation energy density and the number of shots are 700 μ J/cm^2 and 18000, respectively.

4.5 Conclusion

We have been successful in synthesizing CdS quantum dots doped with Mn^{2+} by the aqueous chemical method. The quantum confinement effects on the optical properties of manganese doped CdS quantum dots are studied by means of absorption, PL and PLE spectra as well as luminescence decay at 2 K and room temperature. The main conclusions are:

① The absorption spectra of CdS:Mn quantum dots show the blue shift due to the quantum confinement effect. However, no absorption band of Mn^{2+} cations was observed because of the low Mn^{2+} doping concentrations.

② The strong Mn^{2+} emission band associated with the 3d electron $^4T_1 - ^6A_1$ transition was observed, and it decays fast with the lifetime in ns regime.

③ PLE observations show Mn^{2+} emission is excited through the energy transfer from the host CdS quantum dots to the internal Mn^{2+} levels.

These properties of Mn^{2+} emission are explained based on the interaction of s-p electrons of the host CdS quantum dots with the d-electrons of the doping Mn^{2+} cations.

References

[1] R. N. Bhargava, D. Gallagher, X. Hong and A. Nurmikko, *Phys. Rev. Lett.* 72, 416 (1994).

[2] M. A. Chamarro, V. Voliotis, R. Grousson, P. Lavallard, T. Gacoin, G. Counio, J. P. Boilot and R. Cases, *J. Crystal Growth* 159, 853 (1996).

[3] C. V. Bindhu, S. S. Harilal, G. K. Varier, R. C. Issac, V. P. N. Nampoori, C. P. G. Vallabhan, *J. Phys. D, Appl. Phys.* 29 (4) 1074-9 (1996).

[4] M. Ikeda, K. Itoh and H. Sato, *J. Phys. Soc. Japan* 25,455 (1968).

[5] L. E. Brus, *Appl. Phys.* A53, 465 (1991).

[6] A. D. Yoffe, *Adv. Phys.* 42, 173 (1993).

[7] O. Goedee, W. Heimbrodt, M. Lamla and V. Weinhold, *Phys. stat. sol.* b 146, K65 (1988).

[8] C. Ehrlich, W. Busse, H. E. Gumlich and D. Tschierse, *J. Crystal Growth* 72, 371 (1985).

[9] H. Ito, T. Takano, T. Kuroda, F. Minami and H. Akinage, *Proc. 2nd Asia Sym. Cond. Mat. Photophys.* 365 (Nara, 1996).

[10] A. A. Khosravi, M. Kundu, L. Jatwa, S. K. Deshpande, U. A. Bhagwat, M. Sastry, S. K. Kulkarni, *Appl. Phys. Lett.* 67, 2702 (1995).

[11] M. A. Hines and P. Guyot-Sionnest, *J. Phys. Chem.* 100, 468-471 (1996).

[12] S. A. Blanton, A. Dehestani, P. C. Lin, P. Guyoy-Sionnest, *Chem. Phys. Lett.* 229, 317 (1994).

[13] S. A. Empedocles, D. J. Norris and M. G. Bawendi, *Phys. Rev. Lett.* 77, 3873 (1996).

[14] T. Yoshiue, H. Iwata, M. Kobayashi, Y. Kobayashi, S. Endo, *Proc. 2nd Asia Sym. Cond. Mat. Photophys.* 365 (Nara, 1996).

[15] C. Falcony, M. Garcia, A. Ortiz and J. C. Alonso, *J. Appl. Phys.* 72 (4), 1525 (1992).

[16] A. A. Khosravi, M. Kundu, B. A. Kuruvilla, G. S. Shekhawat, R. P. Gupta, A. K. Sharma, P. D. Vyas and S. K. Kulkarni, *Appl. Phys. Lett.* 67, 2506 (1995).

[17] K. Sooklal, B. S. Cullum, S. M. Angel and C. J. Murphy, *J. Phys. Chem.* 100, 4551 (1996).

[18] Y. L. Soo, Z. H. Ming, S. W. Huang, Y. H. Kao, R. N. Bhargava and D. Gallagher, *Phys. Rev.* B50, 7602 (1994).

[19] D. Dexter, *J. Chem. Phys.* 21, 836 (1953).

[20] Th. Förster: *Ann. Physik* 2, 55 (1948).

5 Conclusion and remarks

5.1 Conclusion

In this paper, we present the experimental studies on the optical properties of II-VI semiconductor quantum dots embedded in the polymer matrix. The obtained results are summarized as:

① We succeeded in preparing the CdS and CdS:Mn quantum dots embedded in polyvinyl alcohol (PVA) matrix by the chemical methods.

② We first studied the PSHB phenomena in CdS quantum dots embedded in the polymer matrix and found its persistent time depends on the molar rate of Cd^{2+}/S^{2-} in the sample. It was found that the persistent time of burnt hole is less than 0.33 ms when Cd^{2+}/S^{2-} less than 1, less than 0.1 sec when Cd^{2+}/S^{2-} near 1, and larger than 1 min when Cd^{2+}/S^{2-} larger than 1.

③ We proposed the photoionization of quantum dots to explain the PSHB phenomena. An electron escapes from the quantum dot through the potential barrier in the polymeric host and is trapped at Cd^{2+} center in the polymeric host. Photoionized quantum dots and trapped electrons are stable enough to give PSHB at low temperature. There are many spatial arrangements for electrons and holes in both quantum dots and the polymeric host. A variety of spatial arrangements induce an additional inhomogeneous broadening of the absorption spectra of CdS quantum dot. The presence of the inhomogeneous broadening coming from the carrier distribution satisfies the requirement of the PSHB.

④ In the CdS:Mn quantum dots, the blue shifted absorption due to the quantum size effect was observed. No obvious absorption band of

Mn^{2+} cations in CdS:Mn quantum dots was observed.

⑤ The photoluminescence of Mn^{2+} in CdS:Mn quantum dots with a large quantum yield and the short lifetime of nanosecond order was observed.

⑥ From the photoluminescence excitation spectrum, we found that the Mn^{2+} is excited through the energy transfer from CdS.

⑦ Mn^{2+} photoluminescence comes from the $^4T_1 - {}^6A_1$ transition of the Mn^{2+} ions in the CdS:Mn quantum dots, but not from the Mn^{2+} ions located in the PVA matrix and on the CdS dot surface.

⑧ Large spatial overlap of the exciton states of CdS with the d-electron state of Mn^{2+} makes the energy transfer rate from CdS to Mn^{2+} increased through the exchange interaction of 3d-electrons of Mn^{2+} ions with the CdS s,p electrons (holes) and the enhanced electric multipole interaction (dipole-dipole, dipole-quadrupole) between the exciton and 3d-electrons of Mn^{2+} ions. The enhanced s, p-d interaction in CdS:Mn quantum dots also relaxes the partial spin-forbidden transition of Mn^{2+}, and results in fast decay time of Mn^{2+}.

⑨ The high quantum yields of Mn^{2+} emission are explained by the combined effects, i.e.

(a) The surface passivation by MnS, $Cd(OH)_2$, $Mn(OH)_2$ and PVA. The surface of quantum dots may be passivated. Then the nonradiative energy transfer rate to the surface trap centers is decreased, and this results in the high quantum yields of Mn^{2+} emission.

(b) The increase of energy transfer rate.

(c) The short lifetime of Mn^{2+} ion emissions.

However, since there is little knowledge on optical properties of

CdS:Mn DMS quantum dots synthesized by the organmetallic methods,* there still exist some questions related to this work and should be studied further. We list them in the following,

① The transfer rate to the Mn^{2+}.

② The nature of Mn^{2+} excited state: how to explain the broad structure and the non-single exponential decay of Mn^{2+} emission, what kind of affection from the surface atomic groups, charges to the Mn^{2+} cations in the quantum dot.

③ How to characterize the doping impurity atoms in quasi-zero structure, e.g., their concentration, local structure.

④ Whether the exciton magnetic polaron theory can be applied to the wide band gap DMS (e.g., ZnS:Mn and CdS:Mn) quantum dots or not.

⑤ The theoretical studies on the Mn^{2+} luminescence behaviors in the wide band gap DMS (e.g., ZnS:Mn and CdS:Mn) quantum dots.

5.2 Future remarks

The science of quantum dots has greatly progressed in the past decade. We can expect steady improvements in the future years in the

---

* According author's knowledge, there are only two research paper published dealing with CdS:Mn quantum dots; one is about chemical synthesis method [R. J. Bandaranayake, M. Smith, J. Y. Lin, H. X. Jiang and C. M. Sorensen, *IEEE Trans. Mag.* 30, 4930 (1994).], the other one showed different observations with this research [M. A. Chamarro, V. Voliotis, R. Grousson, P. Lavallard, T. Gacoin, G. Counio, J. P. Boilot and R. Cases, *J. Crystal Growth* 159, 853 (1996).]; in fact, the research on the optical properties of the bulk $Cd_{1-x}Mn_xS$ mixed crystal is also very few comparing to $Cd_{1-x}Mn_xTe$ and $Zn_{1-x}Mn_xS$.

study of quantum dot materials, because good quality samples will be available. The quantum dots incorporated with magnetic atoms, or the hybrid quantum structure may be studied further especially in the electric field and magnetic field. The novel optical properties and magneto-optical properties in these materials may find their ways applied to the new concept devices. New generation experiments, e. g., single quantum dot spectrum measurements, may be a good method to study quantum dots.

Acknowledgments

The author expresses a deep sense of gratitude to Professor Yasuaki Masumoto for the constant guidance and encouragement throughout this work. The author is indebted to Dr. Tsuyoshi Okuno for the technical helps in operating a fs laser system and useful discussions. The author express sincere thanks to Dr. Yoshihiko Kanemitsu and Dr. Tomobumi Mishina for encouragement and discussions.

The author would like to thank all members of the research group of Prof. Masumoto, especially Dr. Shinji Okamoto, Dr. Tadashi Kawazoe and Mr. Jialong Zhao for their technical helps and discussions.

The small angle X-ray scattering experiments were done at Photon Factory (PF), KEK. The author wishes to thank Prof. Y. Amemiya in PF for his guidance to the small angle X-ray scattering experiments.

Appendix A List of symbols

a_B	bulk exciton Bohr radius
E_b	bulk exciton binding energy (equal to E_R)
E_g	band gap energy for bulk semiconductor
E_R	bulk exciton Rydberg energy (equal to E_b)
f	oscillator strength
m_e^*	electron effective mass
m_h^*	hole effective mass
m_0	free electron mass
M	$m_e^* + m_h^*$, exciton mass
R	nanocrystallite radius
α	absorption coefficient
$-\Delta\alpha$	differential absorption coefficient, given by $-\Delta\alpha = \alpha_1 - \alpha_2$
ε_1	dielectric constant of matrix
ε_2	dielectric constant of nanocrystallite
μ	reduced exciton mass, given by $1/\mu = 1/m_e^* + 1/m_h^*$
P_{DA}	probability of energy transfer between a pair of donor and acceptor

Appendix B List of publications

On optical properties of II-VI compound semiconductors

1. Optical Properties of CdS:Mn nanocrystal in Polyvinyl Alcohol
   Jifa Qi, Tsuyoshi Okuno and Yasuaki Masumoto
   Proceedings of 2 nd Asia Symposium on Optical Properties of Condensed Matter (1996, Nara, Japan) 333.
2. Spectral Hole Burning in CdS Nanocrystals Embedded in Polyvinyl Alcohol
   Jifa Qi and Yasuaki Masumoto
   Solid State Communications **99**, 467 (1996).